AD_____

Award Number:

W81XWH-11-1-0752

TITLE:

Mechanism and therapy for the shared susceptibility to migraine and epilepsy after traumatic brain injury (TBI).

PRINCIPAL INVESTIGATOR:

K.C. Brennan M.D.

CONTRACTING ORGANIZATION:
University of Utah, Salt Lake City UT 84108

REPORT DATE:

October 2013

TYPE OF REPORT:

Annual

PREPARED FOR:

U.S. Army Medical Research and Materiel Command, Fort Detrick, Maryland 21702-5012

DISTRIBUTION STATEMENT:

Approved for Public Release; Distribution Unlimited

REPORT DOCUMENTATION PAGE

Form Approved
OMB No. 0704-0188

1. REPORT DATE	2. REPORT TYPE	3. DATES COVERED
October 2013	Annual	30September2012–29September2013

4. TITLE AND SUBTITLE
Mechanism and therapy for the shared susceptibility to migraine and epilepsy after traumatic brain injury.

5a. CONTRACT NUMBER

5b. GRANT NUMBER
W81XWH-11-1-0752

5c. PROGRAM ELEMENT NUMBER

6. AUTHOR(S)
KC Brennan, Ed Dudek, Wendy Pouliot, Jorge Manuel Mendez, Punam Sawant.

E-Mail: k.c.brennan@hsc.utah.edu

5d. PROJECT NUMBER

5e. TASK NUMBER

5f. WORK UNIT NUMBER

7. PERFORMING ORGANIZATION NAME(S) AND ADDRESS(ES)

AND ADDRESS(ES) University of Utah
383 Colorow Drive, Room 364
Salt Lake City UT 84108

8. PERFORMING ORGANIZATION REPORT NUMBER

9. SPONSORING / MONITORING AGENCY NAME(S) AND ADDRESS(ES)
U.S. Army Medical Research and Materiel Command
Fort Detrick, Maryland 21702-5012

10. SPONSOR/MONITOR'S ACRONYM(S)

11. SPONSOR/MONITOR'S REPORT NUMBER(S)

12. DISTRIBUTION / AVAILABILITY STATEMENT
Approved for Public Release; Distribution Unlimited

13. SUPPLEMENTARY NOTES

14. ABSTRACT

Our proposal studies the natural history and mechanisms of increased brain excitability leading to migraine and epilepsy after traumatic brain injury. In the 18 months since this grant was funded, we have performed experiments spanning nearly the whole range of our proposed work. The most important milestones in this project year have been: 1. Successful implementation of very challenging *post-TBI in vivo* two-photon imaging and *in vivo* whole cell recording. 2. Identification of *novel TBI-specific phenotypes* from our *in vivo* whole cell recordings. 3. Resolution of technical difficulties in telemetry recordings, and recording of both acute and chronic datasets. 4. Progressive implementation of histological techniques, with confirmation thus far of expected TBI phenotypes. 5. Implementation of post-TBI pain behavior measurements.

15. SUBJECT TERMS
Traumatic brain injury, cortical spreading depression, seizure, post-traumatic headache, post-traumatic epilepsy, migraine, epilepsy.

16. SECURITY CLASSIFICATION OF:			17. LIMITATION OF ABSTRACT	18. NUMBER OF PAGES	19a. NAME OF RESPONSIBLE PERSON
a. REPORT	b. ABSTRACT	c. THIS PAGE			19b. TELEPHONE NUMBER *(include area code)*
U	U	U	UU	57	USAMRMC

TABLE OF CONTENTS

INTRODUCTION

Despite great improvements in medical care, traumatic brain injury (TBI) remains the leading cause of death in those under 40 years of age[1,2], in both civilian and military populations. Moreover, as protective strategies and acute treatment have improved, TBI survivors are often profoundly affected by the long-term consequences of injury. These long-term consequences include two disorders of altered brain excitability: chronic headache (usually chronic migraine) and epilepsy. Our proposal examines the links between TBI and these two conditions, which themselves are closely related[3] and can occur in the same patient after injury. Our underlying hypothesis is that the shared susceptibility to migraine and epilepsy after TBI is due to a long-term increase in cortical excitability induced by brain trauma.

Specifically:

-We suspect that the secondary injury phase after TBI, characterized by edema, excitation, and profound structural changes, entrains a 'negative' plasticity, which results in long-term aberrant excitation. We test this with prospective monitoring and mechanism-driven experimental manipulation.

-It is our hypothesis that the glial scar serves as a nidus of hyperexcitability even after conventional recovery is complete. We test with video EEG monitoring for increased excitability, and use behavioral measures to test the pain response. We will specifically probe the glial scar and surrounding tissue for evidence of aberrant excitation.

-If development of migraine and epilepsy after TBI is driven by cortical plasticity, modulation of these processes is important, but clinical tolerability is crucial. Memantine is both well tolerated and mechanistically promising; we will test it after CCI as a potential preventive of post-traumatic migraine and epilepsy.

BODY

Task 1. Acute/subacute experiments after controlled cortical impact (CCI) TBI (Brennan, Dudek, Months 1-36)

Dudek Lab CCI Procedure.

Male, C57B1/6 mice (n=29) were anesthetized with 2-4% isofluorane and pretreated with atropine (2 mg/kg), and penicillin (0.2 mL, SC, 300,000 IU). The surgical site was shaved, prepped with betadine scrub and solution and isolated with sterile surgical towels. For the CCI procedure, once the mouse was secured in the stereotaxic unit, a rectal probe was inserted and a rectal temperature of 37 ± 0.5 °C was maintained with a temperature-controlled heating pad. Next, a mid-sagittal skin incision was made from the occipital notch to the forehead. A dental drill was used to perform a 3-mm craniotomy, using bregma, and coronal, lambdoidal, and interparietal sutures as landmarks. A microprobe (Physiotemp) was inserted through a burr hole into the left frontal cortex to monitor brain temperature, which was maintained at 37 ± 0.5 °C by adjusting the warming blanket and warming lights. For the injury 1-mm metal impactor tip was pneumatically driven at a velocity of 4.0 m/s, depth of pentration 1.0 mm and duration of 100 msec to induce the traumatic brain injury. For the EEG recordings 2 holes were drilled into the skull for the support screws and the two wire EEG electrodes placed on the dura over the CCI-injury site. The entire electrode unit was secured to the skull with dental cement. The skin surrounding the electrode base was sutured shut with non-dissolvable suture. Bupivicane (7.5mg/ml, SC) was applied to all surgical sites. Age-matched sham craniotomies served as controls. Shams underwent anesthesia and preparative surgery but no CCI.

Seizures after CCI TBI.

To continue testing the hypothesis that acute seizures following a traumatic brain injury may be a predisposing factor for the development of PTE, we subjected mice (n=15) to a moderately severe CCI injury. Immediately after the impact, the mice were implanted with a wireless EEG telemetry device. To serve as a control, sham-operated mice (n=14) underwent the same surgical procedures but were not injured. Video-EEG data were collected continuously for 90 days. To date, we have analyzed 30 of the 90 days of video-EEG recordings. Thus far, we have recorded spontaneous seizures in 26% (4/15) of the CCI-injured mice. Nine hours post-injury, one mouse developed status epilepticus (**Figure 1**) which continued for 3 days resulting in the animal's death. Spontaneous recurrent seizures were recorded in 3 other CCI-injured mice (**Figure 2**). For the CCI-injured mice, the average seizure frequency was 0.10 seizures per day.

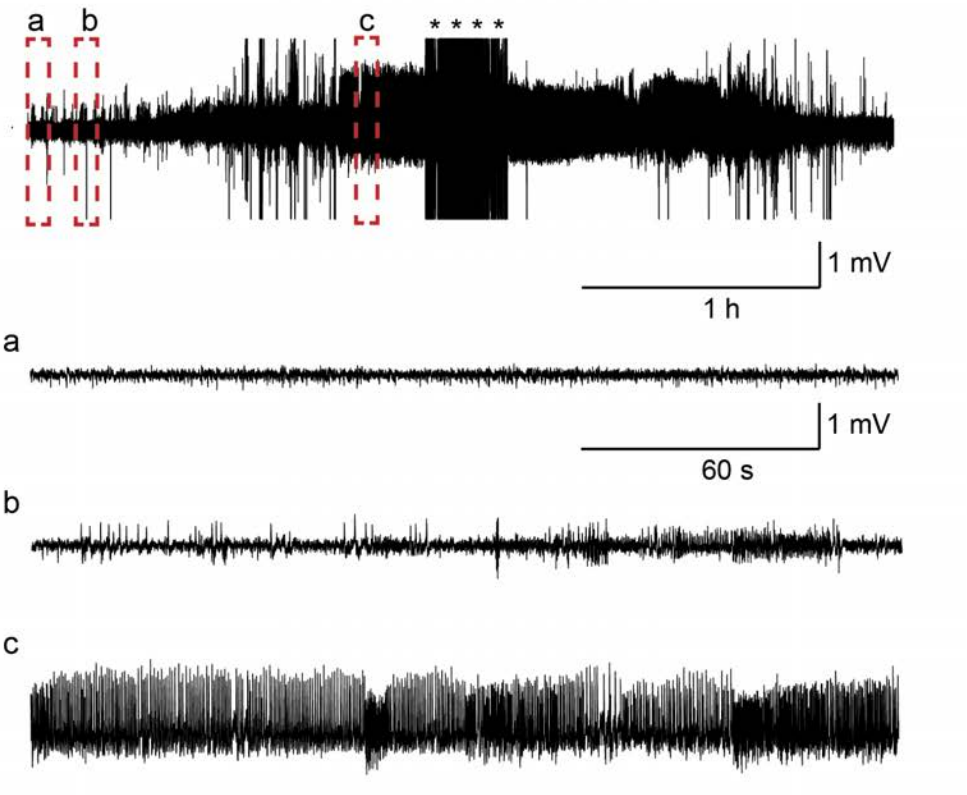

Figure 1: *Electrographic recording of a CCI-injured mouse in status epilepticus.*
*Upper trace is an EEG recording of 4 h of status epilepticus while the lower traces represent portions of the EEG within the dashed boxes at an expanded timescale. The recordings below demonstrate the baseline EEG (a), an individual seizure (b) and the continuous spiking evident of status epilepticus (c). * represents movement artifact from the seizure motor activity.*

Although we have successfully recorded spontaneous seizures from CCI-injured mice for 90 days, four potential caveats exist. The first is that the incidence of seizures in the CCI-injured mice was low (26%). In order to test the effects of memantine on the development of post-traumatic epilepsy, we may have to increase both the incidence of seizures and seizure frequency in the experimental group. As is evident clinically, the time from the injury to the development of late spontaneous recurrent seizures can be lengthy and variable. In order to maximize our ability to detect late seizures, we can length the time of EEG recordings from 90 to 120 days.

The second caveat is that spontaneous seizures were recorded from 21% of the sham-operated controls (**Figure 3**). Seizure/epileptiform activity in sham-operated controls has been reported by others[4]. Clinically, a risk factor for developing epilepsy is having undergone a craniotomy. Craniotomies themselves can produce neuronal damage[5]. To reduce the incidence of seizures in our control group, we can change our methods for the craniotomy. Currently, we are using a dremel with a round burr attachment to perform the craniotomy. There is evidence to suggest that a stereotaxic mounted trephine with cold-saline irrigation can reduce the amount of neuronal damage resulting from the craniotomy[5]. Therefore, we can implement this new method to reduce the underlying damage from the craniotomy and thus reduce the incidence of seizures in the control group. Alternatively, the control group could include a sham operation without the 3 mm craniotomy.

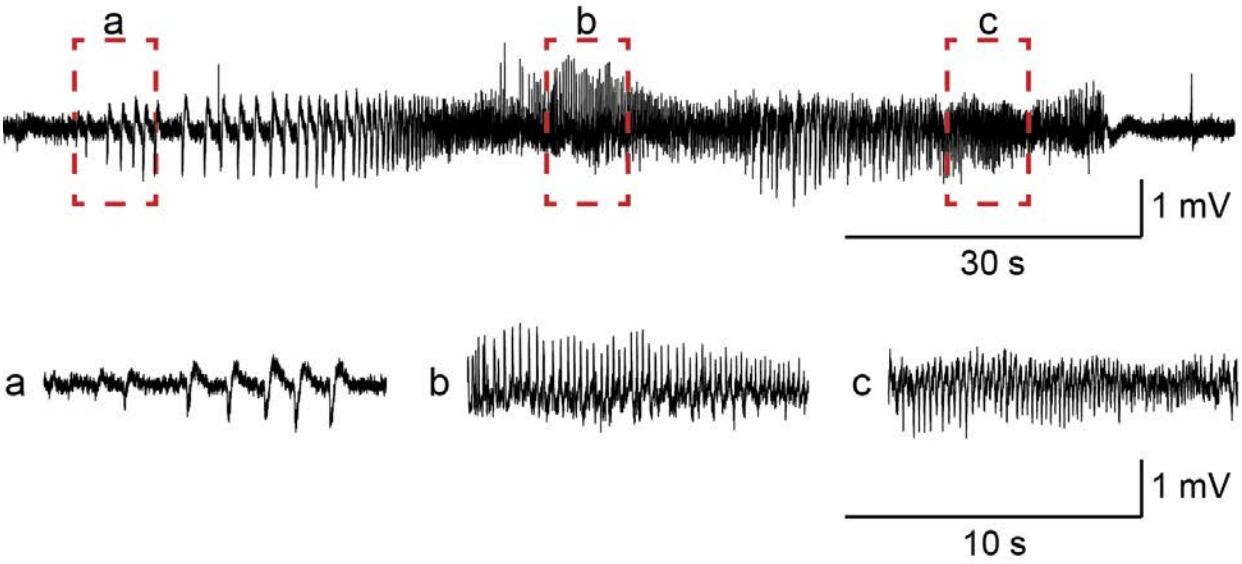

Figure 2: *A spontaneous recurrent seizure in a CCI-injured mouse. An example of an electrographic seizure recorded from a CCI-injured mouse 28 days after the injury. The EEG traces below were selected from the areas highlighted by the dashed boxes. Illustrated in an expanded time scale is the spiking pattern from the beginning (a) middle (b) and end (c) of the seizure.*

The third caveat is that the mortality in the CCI-injured mice was 46%. The majority of the mortality occurs within 1 week following the injury. Although this mortality rate is similar to what has been reported in other TBI studies with moderate-severe injury, we can work to minimize this. To minimize mortality, we can either alter the depth of the injury or adjust the location of the impact.

The fourth caveat is that we lost EEG recordings over time in both the sham-operated and CCI-injured mice (Figure 3). A loss of the EEG recording (33% in the CCI-injured group) resulted from either a loss of the recording electrode from the animal's head or a dead battery in the unit. To minimize the loss of recording electrodes, we can secure the unit to the animal's head with an additional support screw. Although the animals are implanted with units containing a 6-month battery life, the units can fail prematurely. We are working with the supplier to insure that the units will have the appropriate battery life to complete the study.

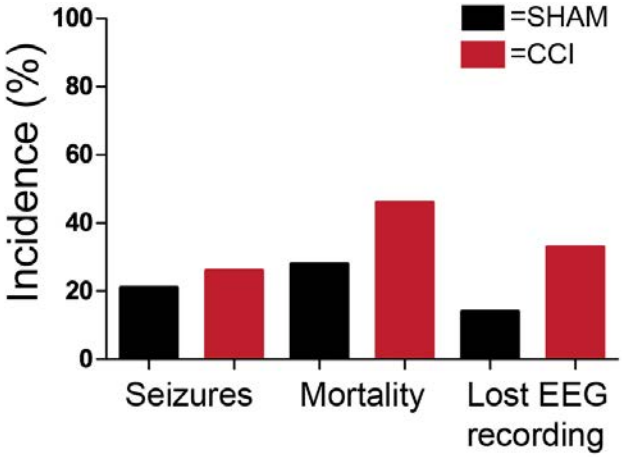

Figure 3: *Bar graph showing the incidence of seizures, mortality and loss of EEG recordings in both the sham-operated controls and CCI-injured mice.*

Seizures and possible cortical spreading depression (CSD) after CCI TBI.

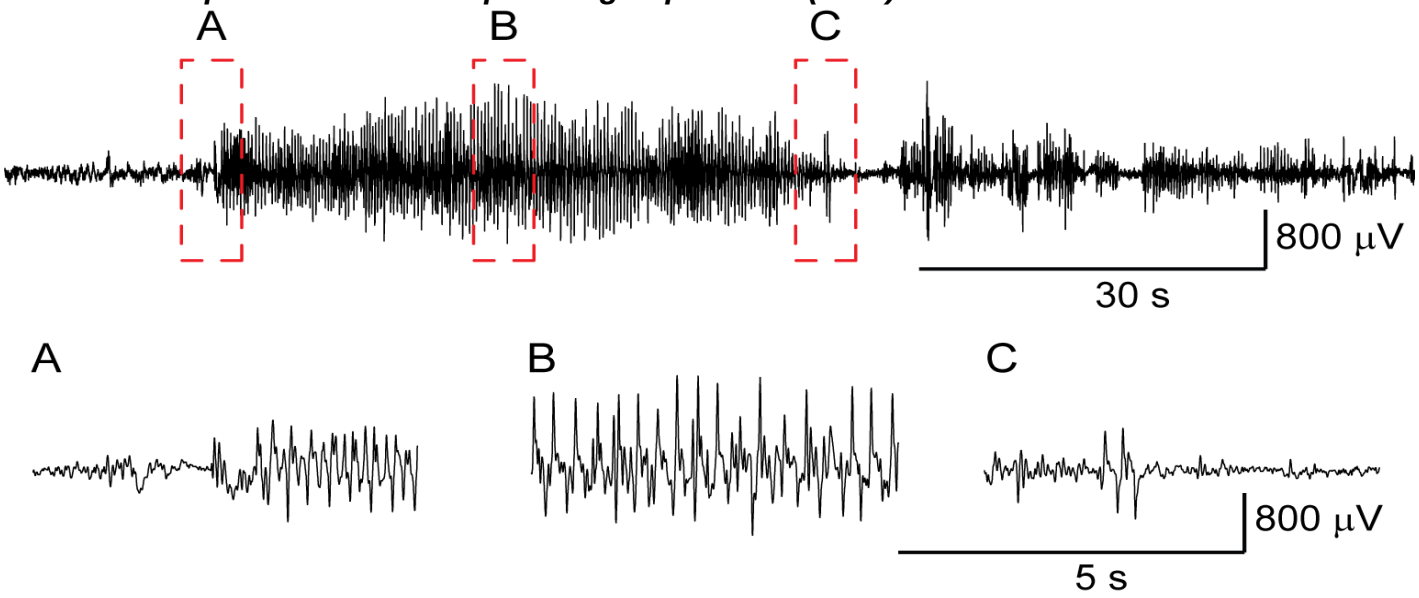

Figure 4: *An example of an electrographic seizure recorded from a CCI-treated rat recorded 3 days post CCI injury. The traces below are expansions of the EEG located in the red dashed boxes. Temporal progression of the beginning (A) middle (B) and end of the seizure (C).*

In a separately funded study we have been recording in rats after CCI. These animals are shown because they demonstrate a long-lasting EEG suppression that resembles what would be seen in an alternating current recording of cortical spreading depression. In this study, experimental animals (n=5) underwent similar CCI procedures to mice, scaled up for rat, while control animals (n=5) underwent a craniotomy and EEG electrode implantation only. Video-EEG data was recorded within 30 min of the injury and for 3-7 days post CCI-injury with a tether-based EEG recording setup. In the majority of the CCI-injured rats, the background EEG signal was suppressed for several hours (see **Figure 4c**). This suppression in background EEG may be caused by spreading depression. Injury-induced seizures were observed in 40% of rats (see **Figure 4a,b**). We are currently analyzing our mouse data to detect this phenotype. Preliminarily, we do not detect it as robustly as in rat; one difference in preparation that may be relevant is that rats were recorded with a tethered system which has a high pass cutoff (low frequency range) broader than the wireless telemetry devices we are using in mice.

Task 1.b. Perform CCI, thresholding for seizure, cortical spreading depression (Brennan, Months 1-24).

Brennan Lab CCI Procedure.

The Leica Impact One steroteaxic impactor [6] was purchased and tested for its reproducibility of impact parameters. The settings used for all experiments thus far have been the following: 4 m/s velocity, 100 ms dwell time, 1 mm impact depth. We have been using a 1 mm diameter flat tipped impactor. So far the device has worked flawlessly, and 2 mm craniotomy surgeries have been very successful (see **Figure 5**). Thus far, 67 animals have undergone CCI; 15 have undergone sham procedure (craniotomy without CCI).

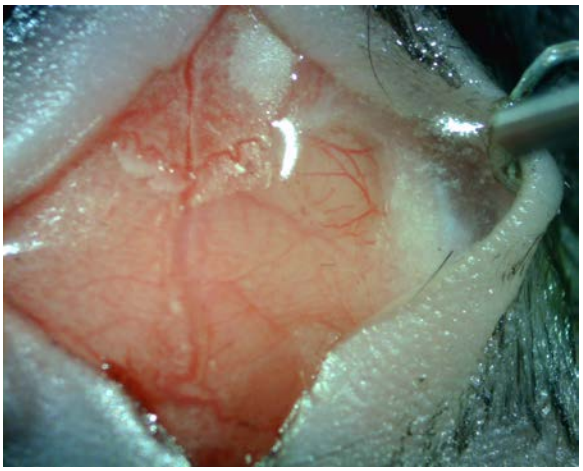

Figure 5: *Typical CCI preparation. Shaved sterilized skin is retracted, 2mm craniotomy is seen to the right of top center, under a saline meniscus. Impactor tip is to the right of the craniotomy. We have performed this CCI procedure in >75 animals so far.*

STAT3 conditional knockout (STAT3-CKO) enhance our mechanistic understanding of TBI effects. Our collaborator Dr. Michael Sofroniew was originally going to provide us with mGFAP-YFP mice, which express yellow fluorescent protein in astrocytes, allowing for specific imaging. These mice have unfortunately been inconsistent in their gene expression. As an alternative Dr. Sofroniew provided us with STAT3-CKO mice. These animals also allow for identification of astrocytes, but have the additional benefit that they allow testing of a signal pathway involved in astrocyte reactivity after TBI. STAT3-CKO mice have selective inactivation of STAT3 in astrocytes through the mGFAP promoter and show disrupted glial scarring and attenuated astrogliosis surrounding spinal cord injury [7]. STAT3 is ubiquitous member of the Jak-STAT signaling family, responsible for the signaling of many cytokines and growth factors [8]. STAT3 is expressed by most cell types in the CNS, and is up-regulated following traumatic brain injury in rodents [9]. The time course of phosphorlyated-STAT3 (activated STAT3) was shown to begin shortly after TBI gaining peak levels around 24 hours, and levels returning to baseline at 7-days, with phosphorylated-STAT3 shown to colocalize predominantly with astrocytes [9]. We are beginning to determine the consequences of selectively ablating STAT3 signaling in astrocytes in relation to TBI and cortical excitability, while simultaneously observing the response in the normal astrocytes of wild-type littermates. This tool significantly amplifies the mechanistic power of our proposal. However the cost of additional animals or experiments (specifically those involving STAT3 transgenic animals; wild-type animal experiments are as we proposed initially) has not and will not be borne by CDMRP as STAT3 mice were not in the original proposal.

Thresholding for seizure and spreading depression after CCI. CSD susceptibility was measured 48 hours and 7 days following injury. The CSD susceptibility procedure consists of re-opening the now fully healed suture in the anesthetized animal to expose the top of the skull. Carefully placed burr holes (being very cautious not to disrupt the dura matter) are placed in both the injured (ipsilateral) and uninjured (contralateral) hemispheres. Microcapillary tips are placed inside the burr holes producing a constant flow (~3.2 ul/min) of 0.9% saline to start. The animal's vital signs and temperature are monitored throughout the surgery. A thin layer of silicone oil is applied to the top of the skull to enhance visibility through the skull. Approximately 15 minutes of images taken with a CCD camera using 535 nm LED illumination (a wavelength that increases hemoglobin contrast) are acquired before the solution perfusing the burrhole is switched to 1 M KCl to induce CSD events. **Figure 6** displays the preparation. Difference images highlight the reflectance changes associated with CSD. Regions of interest placed in both hemispheres show the OIS fluctuations from each event, example shown in traces of **Figure 6**. The number of CSD events in both injured and uninjured hemispheres is recorded for approximately 1 hr following the first CSD event. **Figure 7** shows the

results thus far. Interestingly, we see no significant difference in CSD number, ipsilateral or contralateral to CCI, in sham vs. CCI treated animals or in STAT3 transgenic animals vs. controls, at 48 hours and 7 days after CCI. There is however a difference in the phenotype of the elicited CSDs in CCI cortex (not shown): likely because of the dead tissue in the CCI region, there is a significant increase in the number of circling CSD waves. The physiological significance of this finding is as yet unclear; we are developing tools to better analyze these complex datasets.

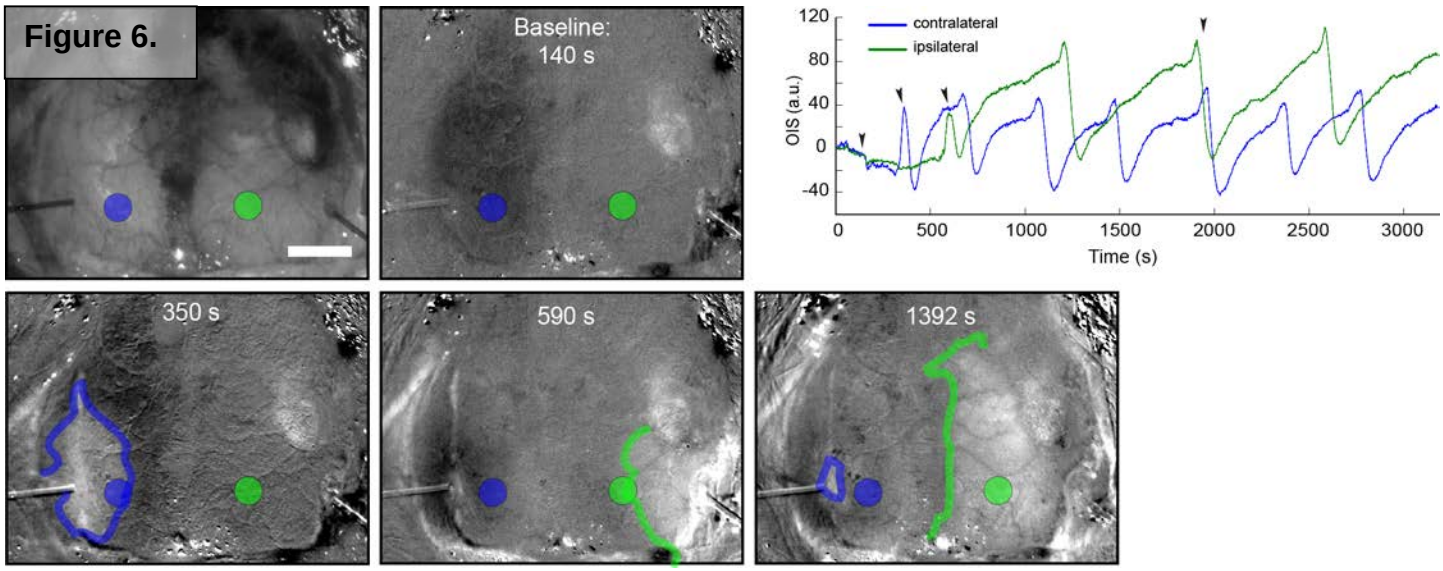

Figure 7.

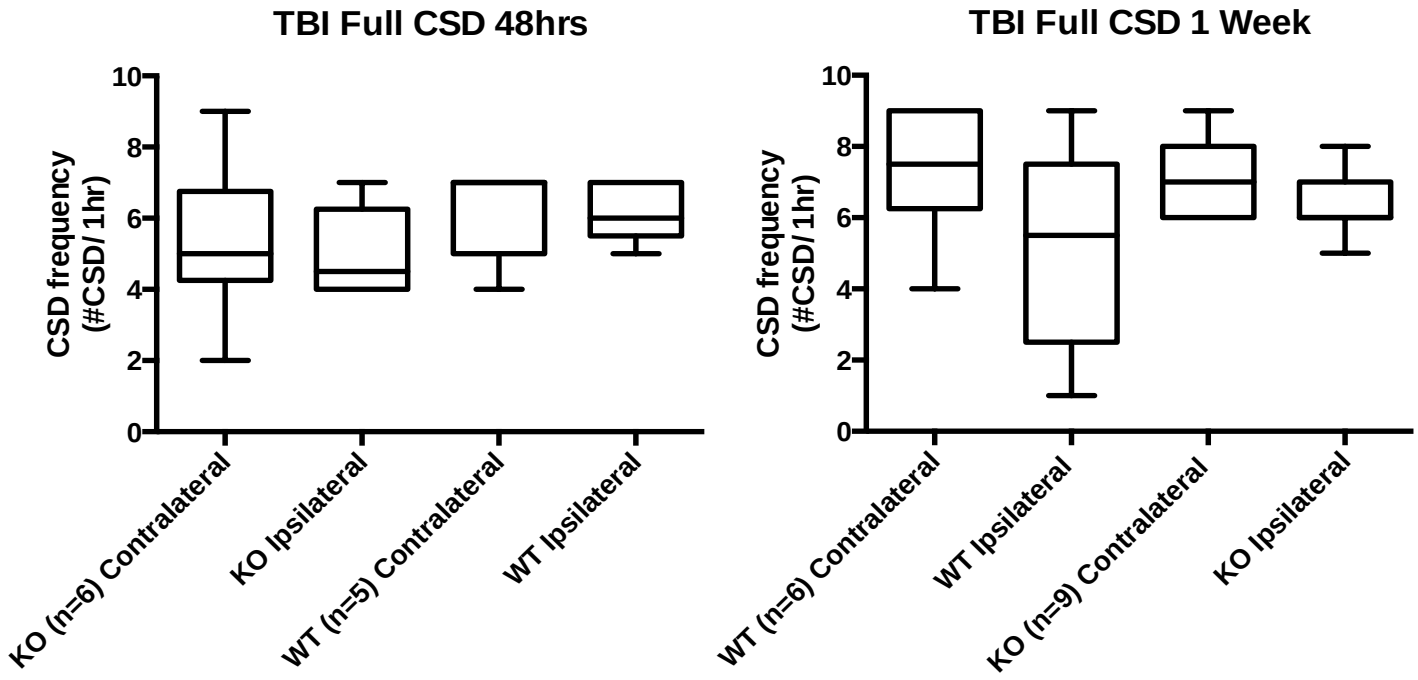

Task 1.c. Perform two-photon experiments 72 hours after CCI (Brennan, Dudek, Months 12-24).

Cell-type-specific labeling and subcellular resolution imaging after TBI.

To uncover the cellular processes involved in TBI, we have developed all necessary two photon microscopy methods, in combination with *in vivo* whole-cell electrophysiology techniques (see below). Two-photon microscopy is used to accomplish longitudinal in vivo studies of anatomical changes and to study changes in calcium dynamics, perfusion, and metabolism. The use of transgenic animals with cell type specific fluorescence, like the GAD67-delta neo mouse, expressing green fluorescent

protein in interneurons, provides the chance to monitor cell-specific changes caused by the TBI experiment. In addition, the use of astrocytic specific dye (SR101) allows the simultaneous inspection of neuronal and astrocytic changes.

Visualization of astrocytes is important to the goals of the grant, and we have tried different techniques to load SR101. The first techniques consisted in loading the astrocytes by loading SR101 topically in the area of the cortex we wanted to visualize, following the methods described in Nimmerjahn et al 2004 [10]. Briefly, a 100µM solution of SR101 in aCSF was applied to a selected exposed area of the cortex. To have a better loading of the dye, the dura matter should be removed or at least perforated and the solution topically applied for 5 minutes and washed away with aCSF. The second technique consisted of tail vein injection of the dye as described in Appaix et al. 2012 [11]. In this case, 20mg/kg of SR101 in physiological solution is tail vein injected. Usually, after half an hour astrocytes are clearly identified. This technique has proven to be more reliable (**Figures 8,9**) and with the convenience of not having to further touch the area of the cortex to be imaged (which can artifactually induce astrocyte reactivity).

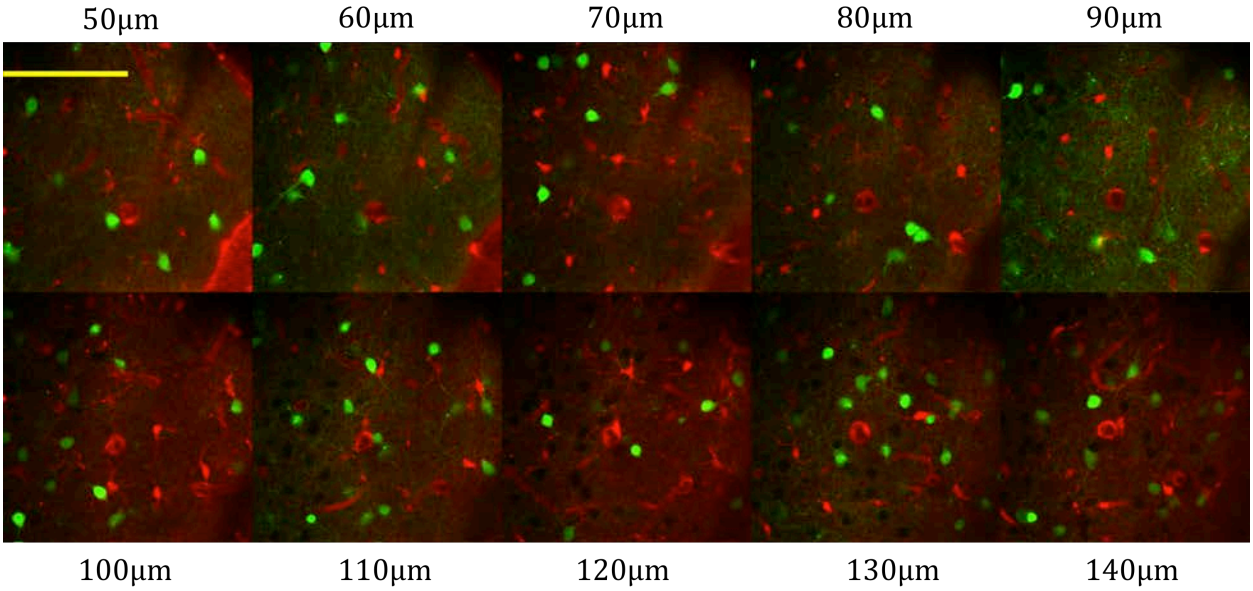

Figure 8: *Two-photon microscope imaging of a GAD67-Δneo mouse with all cortical interneurons identified with GFP and astrocytes stained with SR101. Interneurons are shown in green and astrocytes in red, compatible with fluorophore colors. Though pyramidal neurons are not fluorescent, they are identified by their darker appearance. The scale bar represents 100µm.*

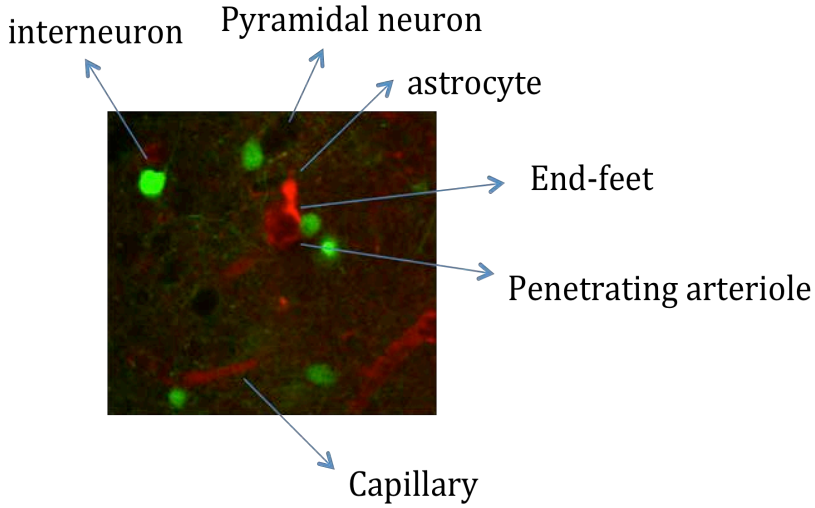

Figure 9: *All the anatomical elements of the network are identified: interneurons, pyramidal neurons, astrocytes and their end-feet, and the vascular components.*

Dendritic beading and cell swelling caused by cortical spreading depression (CSD), which accompanies TBI.

CSD is a massive depolarization that occurs during and after TBI. It causes significant structural and functional changes, including (**Figure 10**) dendritic beading and cellular swelling similar to what is seen during ischemia (except that it appears to be reversible).

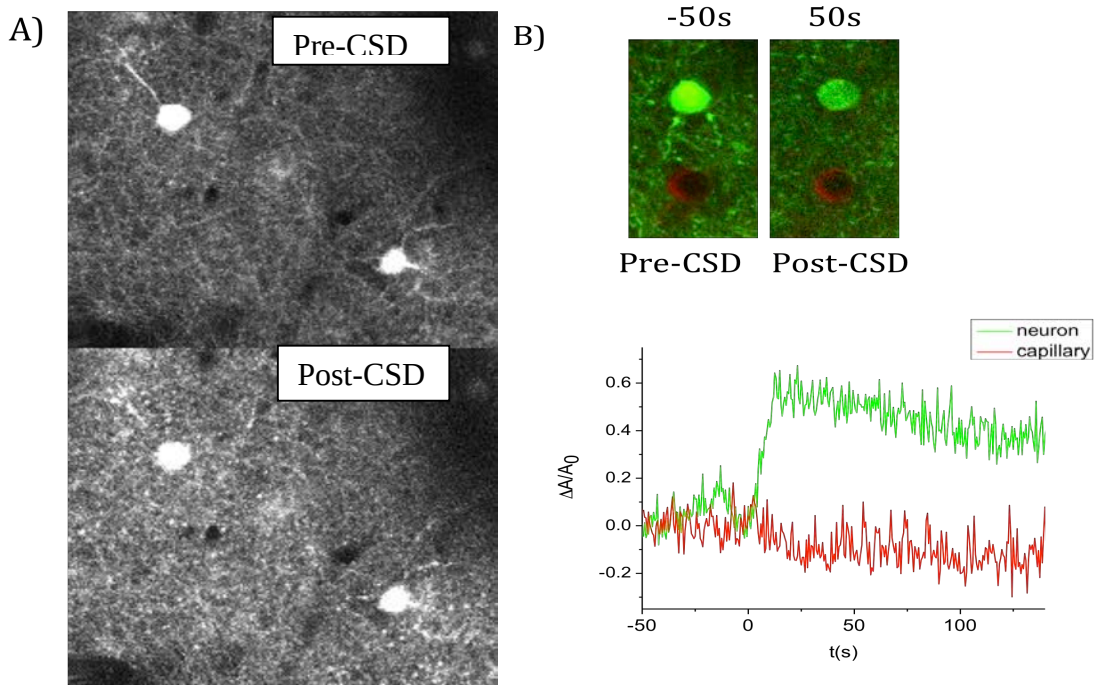

Figure 10: *A) Neuritic beading of the interneurons appears after a CSD event. The beading is visualized as small fluorescent dots in the neural processes. B) Cells swell after CSD. Time traces of the area of the neuron (shown in green) and of a capillary (red) are displayed. The area of the neuron increased more than 50%.*

Alterations in perfusion and metabolism after CSD.

We have implemented methods to monitor blood perfusion and metabolic condition of cortex by two-photon microscopy. By injecting FITC-dextran dyes into the blood a real time quantification of the perfusion is accomplished (**Figure 11a,c**). Detailed imaging of the vessel wall can be obtained with Alexafluor633, which labels elastin filaments (**Figure 11b**). Finally, the intrinsic fluorescence of the cortex can be monitored providing information about the NAD/NADH ratio and thus the tissue metabolism which is ultimately governed by perfusion (**Figure 12**). We have successfully used these techniques to describe changes caused by CSD and are progressively implementing them after CCI (a priority is neuronal recordings and these were done first – see below).

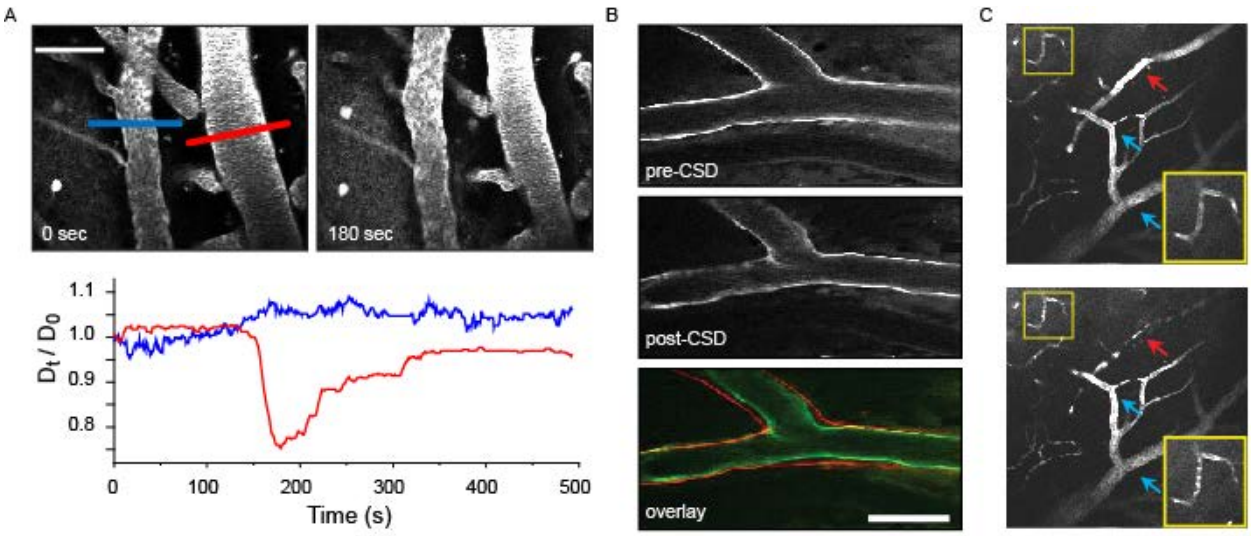

Figure 11: *Massive vascular changes during and after CSD. A. Two photon images of a cortical artery and vein are shown before and during a CSD. Diameter changes were calculated across their cross-section (artery: red, vein: blue) and displayed as time traces in the plot below (scale bar, 50 µm). B. Arteries also undergo morphological changes (labeling of elastin fibers with AlexaFluor 633), becoming more irregular (scale bar, 50 µm). C. Intracortical vascular dynamics during CSD. Images from 50 µm below the cortical surface show penetrating arteriole (red arrow), draining veins (blue arrows) and capillary (yellow inset). Plasma is labeled with 70 kD fluorescein dextran. At baseline, blood flow blurs individual red blood cells (RBCs). During CSD, arteriole (but not vein) constricts massively. Capillary blood flow stops, revealing individual RBCs as dark spots. Shortly after CSD passage, arteriole dilates beyond baseline, but capillary flow is still compromised. Scale: arrows are 50 µm long.*

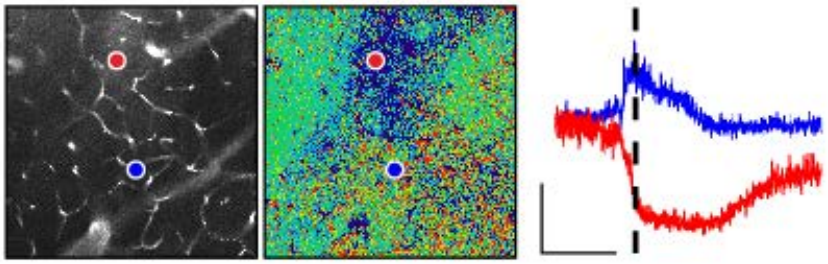

Figure 12: *Fluorescein dextran labeled capillaries 250 µm below the cortical surface (left). NADH intrinsic fluorescence image from same location (center), during peak CSD-associated changes (dashed line on graph). NADH oxidation (red; darkening) and reduction (blue; brightening) can occur, depending on location, however most regions show reduction, consistent with the metabolic challenge of CSD. Calibration: 10% change from baseline; 45 seconds.*

Calcium imaging with Oregon green BAPTA1-AM.

We have implemented calcium imaging of cortical cell populations by bolus loading of Oregon green BAPTA1-AM (OGB). Oregon-Green 488 BAPTA-1 AM is prepared at a concentration of 1 mM. We use a 20% solution of Pluronic F-127 in DMSO and we dissolve 50µg of OGB in it to a concentration of 10 mM. Then this solution is further diluted (to a 1mM solution) in a HEPES aCSF (150mM NaCl, 2.5mM KCl, 10mM Hepes, with a pH of 7.4). The calcium indicator is loaded in a glass pipette and bolus loaded in the cortex at a depth of 200µm (typically using a pressure of 10 PSI for 1 minute) [12]. Imaging is started after an hour of the pressure injections. An example of calcium imaging during CSD event is shown in **Figure 13**. However while is has been useful in uninjured animals, OGB use after TBI has proved problematic; thus we have switched to genetically encoded calcium indicators.

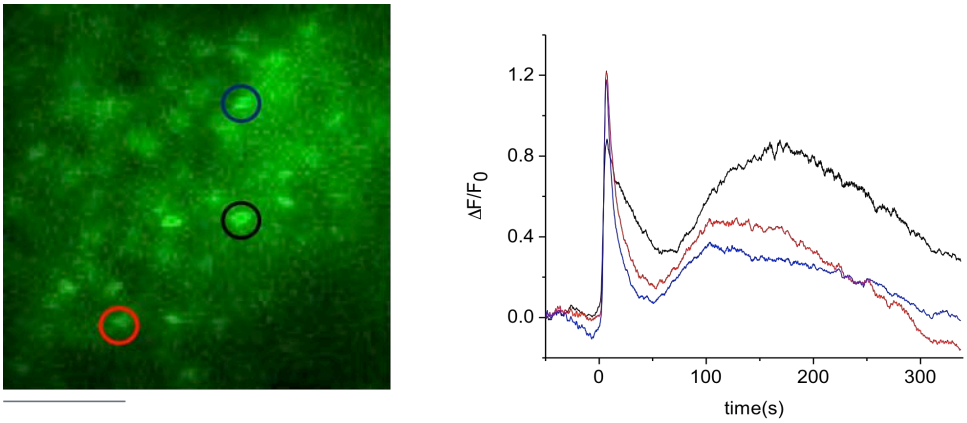

Figure 13. *OGB1 AM loading of a cell population in layer 2/3 of somatosensory cortex (OGB1 selectively labels neurons, but some astrocyte fluorescence is also possible). The fluorescence changes corresponding to the occurrence to a CSD at t=0s in the areas depicted by colored circles are shown in the plot in the right side. The bar indicates 50 µm.*

Imaging with genetically encoded calcium indicators (GECI).

The alternative to dye loading is to use GECI [13,14]. We now routinely use GCaMP5 or 6 delivered by viral vector injections. The use of AAV2/1.hSynap.GCaMP5G(GCaMP3-T302L.R303P.D380Y).WPRE.SV40 reveals neuronal specific population calcium activity in the relevant area of the cortex, because the expression is driven by the neuron-specific Synapsin promoter (**Figure 14**). For this procedure, the animal is anesthetized with isoflurane (5% for induction and 1.5% for the rest of the procedure) and put in the stereotactic apparatus for the correct identification of the region of interest. A small craniotomy is performed, and a small volume (~1 µL) of the virus suspension is loaded in a glass pipette and pressure injected. The craniotomy is sealed with silicone elastomer and the skin reapposed with vetbond. The animal is administered with antibiotics and analgesics and recovered for 2 or 3 weeks to allow for a sufficient expression of GCaMP. After this the animal is prepared for imaging.

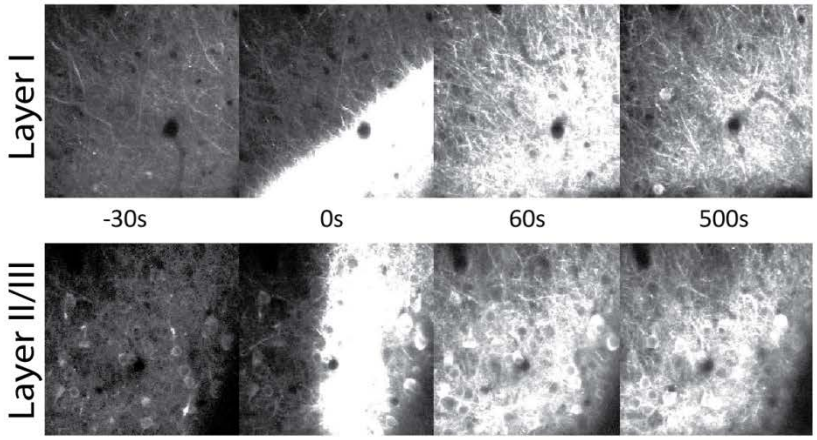

Figure 14: *Layer specific calcium transients in neurons loaded with genetically encoded calcium indicator. An adeno-associated virus encoding GCaMP5 under the synapsin-1 promoter (neuronal specific) was injected in the cortex and 3 weeks later the mouse was prepared for imaging (craniotomy over somatosensory cortex). The same area was imaged at two different depths, corresponding to layer I and layer II/III. Sequences of images show the propagation of the CSD in these two different depths.*

Neuronal two-photon imaging after TBI.

Two photon imaging after TBI has been technically challenging but ultimately successful. We initially used Oregon Green BAPTA multicell bolus loading, where an organic dye is injected acutely during the experiment 72 hours after CCI. Loading (2 animals) was much worse than in non-TBI animals,

with very poor signal. This prompted the use of virus-delivered genetically-encoded calcium indicators. The indicator is injected 2 weeks before CCI in a burrhole 2-3 mm anteromedial to the CCI craniotomy, CCI is delivered, and animals are imaged 72 hours after CCI in a craniotomy between the

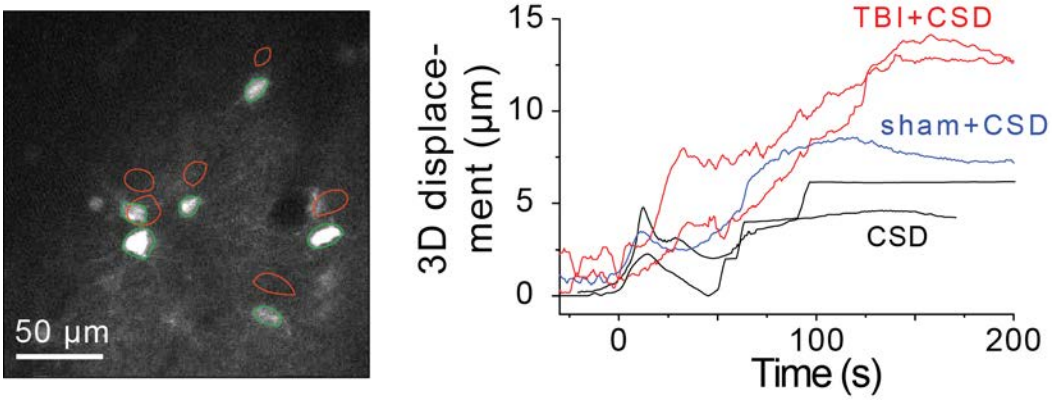

Figure 15. *TBI increases mechanical displacement caused by CSD. Two-photon image (left) shows displacement of GFP labeled interneurons (layer 2/3) in the scanning plane for an animal 48 h after CCI TBI. CSD was induced by topical application of KCl. Red: pre-CSD position; Green: post-CSD position. Plot shows Euclidean distance calculated by a correlation-based algorithm for different animals. Red: mice with TBI 48 h before experimentally induced CSD; Blue: Sham TBI 48 h prior to CSD. Black: Mice with no TBI procedure.*

burrhole and the CCI craniotomy. Of 17 experiments so far with AAV-delivered GCaMP5 as the indicator, 9 have been successful, in that there is good functional signal-to-noise, proper cytoplasmic but not nuclear loading of the dye (see **Figure 14**), and excellent delineation of anatomy. The majority of the 8 unsuccessful experiments were initial trials; success rate has improved with time. And many of the 'unsuccessful' experiments still yield useful data – e.g. good calcium signal but relatively poorer anatomical resolution. **Figure 15** shows increased tissue displacement associated with CSD in a post-TBI animal. Preliminarily we also observe more variable calcium transients, with a significantly greater variance in the range of CSD-associated fluorescence amplitudes (not shown; analysis ongoing).

Astrocyte-specific calcium imaging.

We are interested in understanding the astrocytic changes related to TBI. The use of Fluo4-AM yields astrocytic specific calcium signal (a functional signal as opposed to SR101 which does not change with activity) that can be confirmed with SR-101 labeling [10,12,15]. We have successfully used this dye in WT and in STAT3-CKO animals. The dye loading method was based on the methods described by Hirase et al 2004 [15].

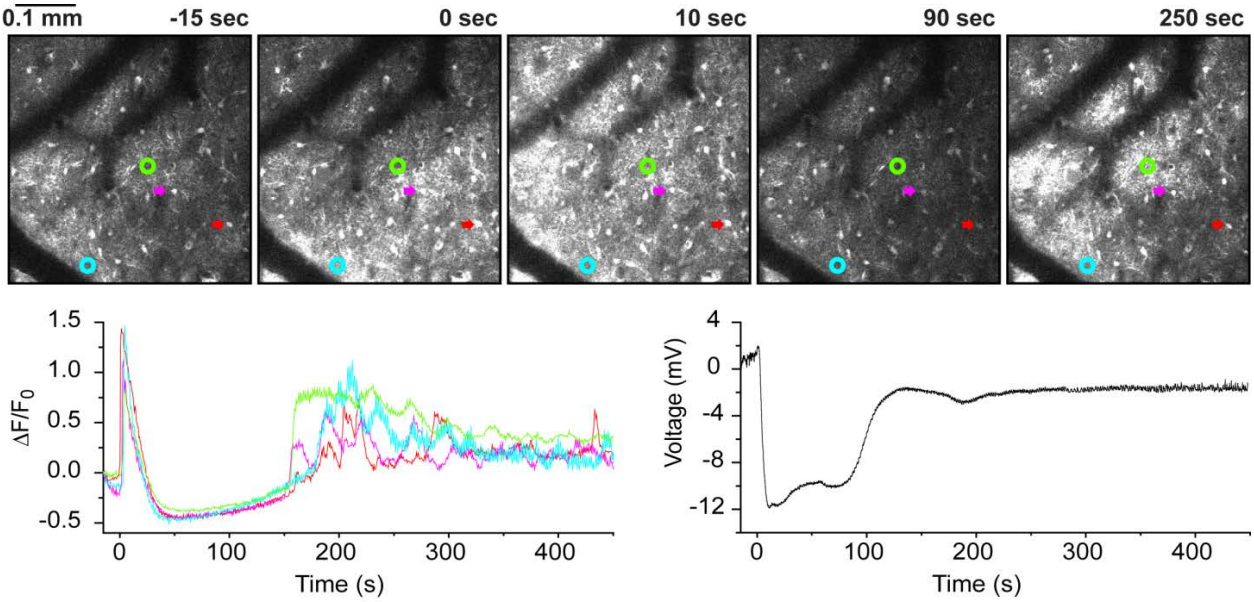

Figure 16: *Massive changes in astrocyte calcium activity during and after CSD. Fluo4-AM was used to load astrocytes in the somatosensory cortex of a WT mouse.* ***A.*** *Time sequence showing the propagation and aftermath of CSD. The wave propagates through the imaging window at 0 s. Colored arrows represent astrocytes and circles represent neuropil. Imaging depth 100 µm.* ***B.*** *Time traces of the fluorescent changes of the astrocytes and neuropil indicated in A. There is a massive increase in astrocyte calcium activity during the wave, followed by a decrease then a subsequent increase to beyond baseline. There is a persistent increase in rhythmic calcium activity. Right hand trace shows field potential deflection associated with CSD, and sustained depolarization after the wave (field potential does not return to baseline) which corresponds temporally with increased calcium activity.*

In vivo *whole cell recording to determine the mechanisms of increased cortical excitability after TBI.*

To study functional changes in cortical neurons after traumatic brain injury, we have used *in vivo* whole cell electrophysiological recordings[16,17]. These recordings will be essential to directly demonstrate synaptic activity associated with sensory processing and behavior.

Surgical Preparation.

Mice (n = 27 to date) were anesthetized using intraperitoneal injection of urethane (1.2- 1.5 g/kg). Body temperature is controlled using a heating pad and maintained at 37°C throughout the experiment. A round craniotomy (approx. 2 mm in diameter) is made in the barrel cortex region (3-4 mm lateral to the midline and 1-2 mm posterior to the bregma). Dura is removed using a 30 gauge syringe needle and fine forceps. Durectomy with less bleeding has been an important step in order to have a clean passage for patch electrode through the tissue. Agar (1%) is placed on the brain surface to keep the surface moist.

Electrophysiological Recordings.

Intracellular recordings are performed using thick-wall glass pipettes pulled from borosilicate glass capillaries (OD 1.65 mm, ID 1.2 mm, Garner Glass, Claremont, CA) with a P-87 Flaming-Brown puller (Sutter Instruments, Novato, CA). Patch electrodes of 5-7 MΩ are used (tip size of 3-4 µm). A patch pipette is filled with intracellular solution containing (in mM; pH = 7.2): 120 K-gluconate, 1 NaCl, 5 EGTA, 10 HEPES, 1 $MgCl_2$, 130 CsCl, 1 $CaCl_2$, 2 ATP, 0.05 mM Alexa 594 (for visualized experiments). Signals are amplified using a Multiclamp 700B amplifier (Axon Instruments, Foster city, CA). Signals are sampled at 10 kHz and low-passed filtered at 2 kHz. Data are acquired and stored on a PC using a Digidata-1320A digitizer (Clampex, Molecular Device, Union City, CA), and pClamp 8.2 software (Clampex, Molecular Device, Union City, CA). Electrode is placed on the surface with positive pressure of 30 kPa and advanced to a depth of 100-200 µm. Once the electrode is lowered to

the desired cortical depth (layer I-II), pressure is reduced to 4 kPa. In voltage clamp mode, the pipette is moved slowly in steps of 0.04 µm through the layers of the cortex while monitoring the current response to an applied voltage step (10 mV amplitude). We further lower the pipette until we observe a consistent reduction in response amplitude (approx. 50%), which indicates an increase in electrode resistance. Then positive pressure is removed to zero and suction is applied if necessary to get a gigaseal (a greater than giga-ohm series resistance recorded through the electrode). The command potential of -70 mV is applied. Negative pressure is applied to obtain a whole-cell configuration. Sometimes a gigaseal mode is left without perturbing, to perform cell-attached experiments. In the current-clamp mode, we record the spontaneous and evoked activity. Cortical spreading depression is induced by pin-prick and recorded (**Figure 17**).

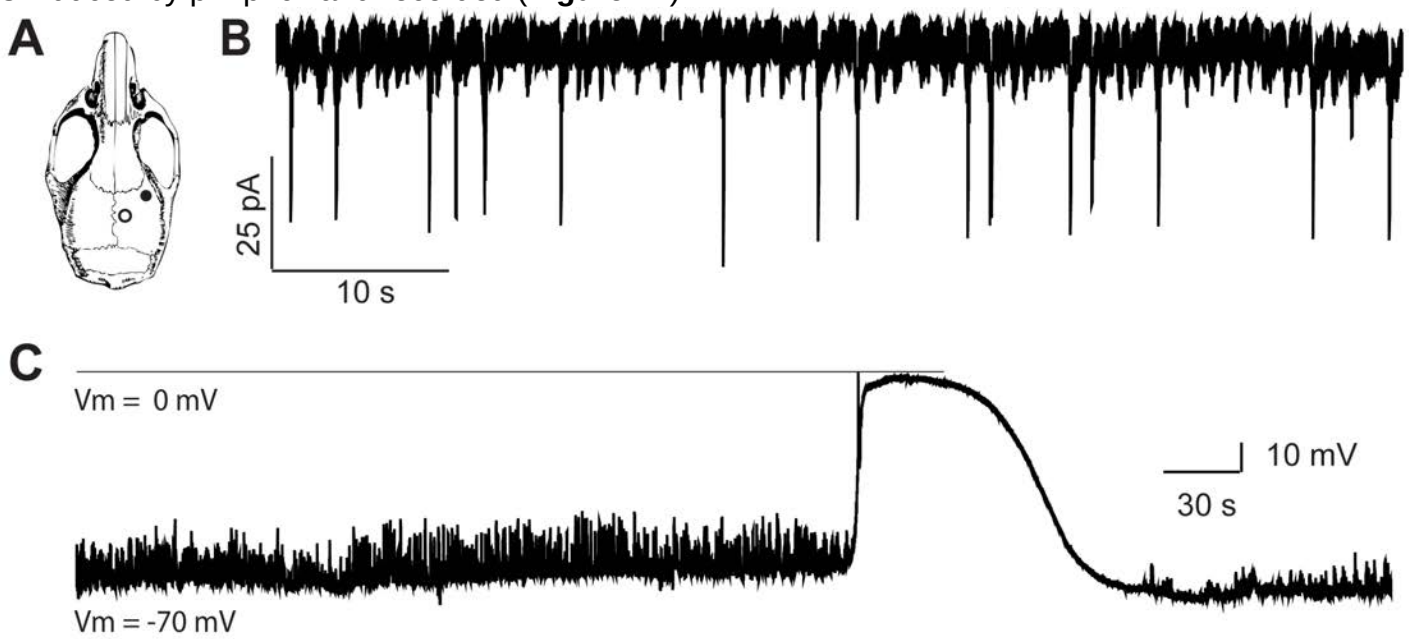

Figure 17: Whole-cell patch clamp recording of CSD in vivo. A. *Schematic representation of the mouse skull demonstrating the location of craniotomy-durectomy for a single-cell recording. Closed and open circles represent locations for electrode placement and CSD induction, respectively.* ***B.*** *Membrane current traces showing spontaneous synaptic activity in layer II somatosensory neurons.* ***C.*** *Membrane potential changes during CSD, measured with patch pipettes filled with K+-gluconate. Following the induction of CSD with pinprick, the membrane potential reached 0mV during the peak of CSD. Note the reduction in neuronal firing after CSD..*

In another set of experiments, we performed visualized whole-cell recordings using two-photon microscopy. Our approach is to use 'shadow patching' technique as described in the grant. Briefly, we eject the fluorescent dye Alexa 594 into the extracellular space. As described by Kitamura et al 2008 [18], individual neurons become visible as dark shadows against the bright fluorescence background. However, in our hands, we were unable to visualize neurons even under high power and different sets of ejection systems. At this stage, we are confident in our skills using blind patch techniques, as well as visualized patch recordings in either GFP or GECI-labelled cells to perform all the experiments outlined in the proposal.

The success rate for whole-cell recordings *in vivo* depends on many factors such as cortical movement, electrode positioning (angle of approach), and the craniotomy preparation. The stability of recordings is mainly associated with breathing and heartbeat-related movements of the animal. Another issue is to obtain seal resistance between the pipette and cell in a giga-ohm range. We were able to reduce cortical motion by preparing small craniotomies. Anesthetics are known to alter the breathing-associated movements so we tried using different compounds such as urethane or isoflurane or a mixture of both. Pure isoflurane results in poor seal quality, and pure urethane is

difficult to control. In our hands, we obtain the fewest artifacts and best anesthetic control with a combination of urethane (0.25 mg/kg, supplemented as necessary) and isoflurane (0.2-0.8 %).

Now that we are obtaining whole-cell recordings in naive animals on a regular basis we have begun testing animals after TBI (n = 27 so far). We collect data from wild-type animals on intrinsic membrane properties, synaptic input during and after sensory, chemical, and electrical stimulation, and cortical spreading depression, in areas near and distant from CCI TBI injury.

We now have datasets that are statistically powered to detect differences after TBI (**Figure 18**). Recordings thus far are within 1 mm of the CCI lesion, or equivalently located by stereotaxic coordinates in sham animals. We find that 72h after TBI, input resistance in putative pyramidal cells is identical between sham and TBI animals. This confirms that recording quality is comparable (and in acceptable range) for both sets and allows relevant comparisons. Membrane potential shows no significant difference, but there is a trend toward a more depolarized potential in TBI animals (for implications see below). In contrast, frequency of spontaneous subthreshold depolarizations and action potentials is significantly reduced in post-TBI animals. There is also a significantly higher rheobase (minimum current needed to elicit action potentials) and decreased input-output curve slope (action potential frequency to increasing current injections) in TBI animals (**Figure 18a,b**). This suggests a reduced excitability in the region surrounding TBI injury, after the event. However, an alternative explanation is that because of a subtly more depolarized membrane potential at baseline, more sodium channels are inactivated in TBI animals. This would result in the identical phenotype to what we observed, but due to an *increase* rather than decrease in excitability. We will be alert to this possibility as we continue our experiments. We will also consider adding brain slice experiments (a proposed alternative approach in our original proposal) if the issue remains uncertain. The cellular environment can be better controlled with brain slices, and should offer more signal-to-noise in making membrane potential comparisons. Whatever the ultimate answer, we have identified a *novel, TBI-specific excitability phenotype* that has mechanistic implications for the development of post-traumatic headache and post-traumatic epilepsy.

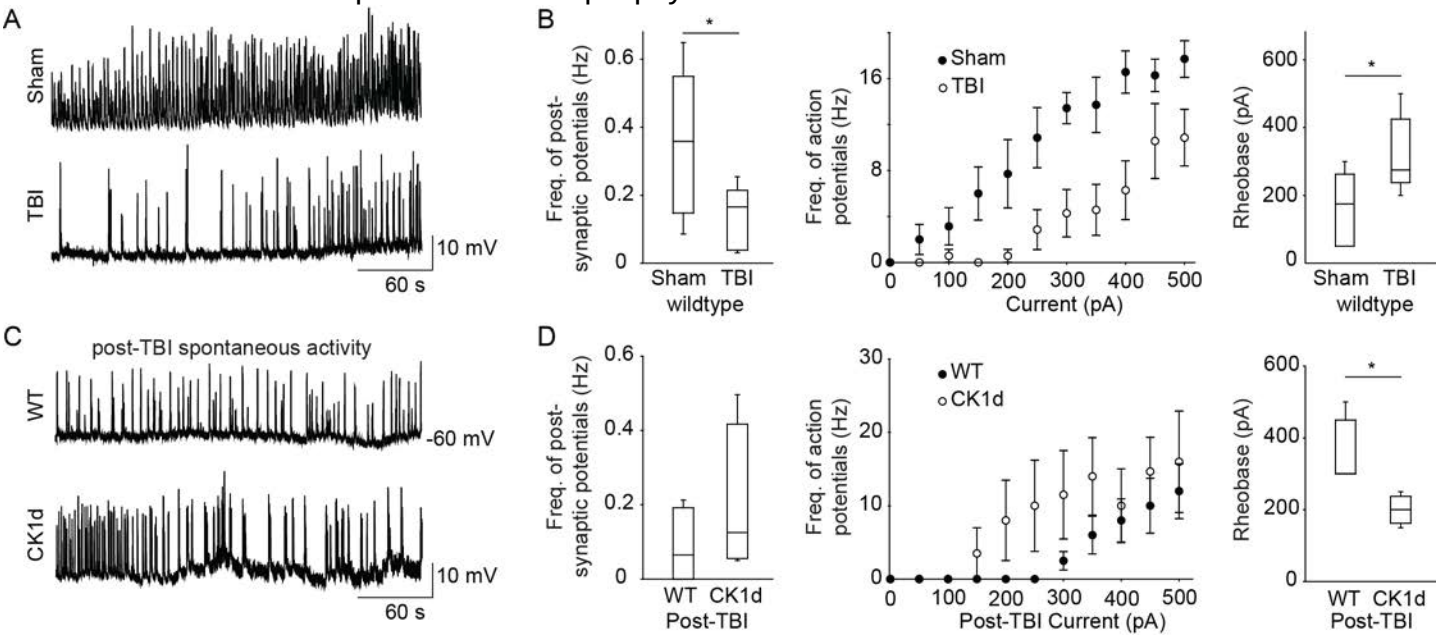

Figure 18: Changes in pyramidal cell excitability after TBI. *In vivo whole-cell current clamp recordings in TBI-injured animals: layer 2/3 pyramidal cells, 48 h after CCI TBI. A. Spontaneous activity recorded from TBI- and sham-treated animals shows reduction in spontaneous synaptic activity 48 h after TBI. B. Principal cells from TBI-lesioned cortex have reduced frequency of sEPSPs (p<0.05, sham: n=8, TBI: n=6) than those from sham-treated animals, suggesting decreased local glutamatergic synaptic connectivity. Input-output curve (action potential frequency to increasing*

current injection) confirms a decreased neuronal excitability after injury, showing (1) a 45% decrease in slope and (2) an 80% increase in rheobase (minimum current needed to elicit action potential). C. Spontaneous activity 48 h after TBI in CK1d mutant and wild-type littermates. D. There is a trend toward increased frequency of synaptic potentials in CK1d mutants. Rheobase is significantly smaller in CK1d animals (p<0.05, sham: n=4, TBI: n=4), but the slopes (frequency of AP's versus current) are not significantly different. Our data suggest a phenotype of increased intrinsic neuronal excitability in CK1d animals that may contribute to neuronal network and circuitry dysfunction following TBI.

Beyond the scope of this grant (separately funded) but very relevant to the post-traumatic headache aims of this proposal, we have also been examining the post-TBI response in animals with a mutation in the casein kinase 1 delta (CK1d) gene. CK1d animals carry a mutation found in familial migraine, and have sensory and physiological characteristics consistent with migraine[19]. It is known that post-traumatic headache is more common in migraineurs[20], thus there may be unique physiological susceptibility characteristics. Interestingly, we find that in contrast to wild-type littermates, CK1d transgenic animals have an *opposite* excitability phenotype after TBI, with a significantly *decreased* rheobase, and trend toward *increased* subthreshold and action potential activity, and *increased* input-output slope (**Figure 18c,d**). While not directly relevant to this proposal, they additionally validate our approach and motivate future post-traumatic headache related work in migraine models.

Task 1.d. Perform two-photon experiments 72 hours after lipopolysaccharide injection, acutely after hypotonic ACSF perfusion (Brennan, Months 18-30).

Figure 19.

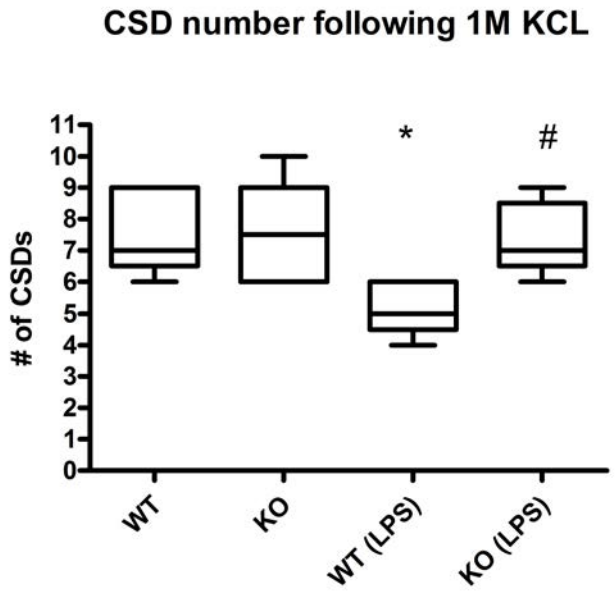

To ascertain the effect of a *low dose LPS injection* on cortical excitability, a group of 22 male animals was used to determine the effect of LPS exposure to CSD threshold. 6 WT and 6 KO animals were initially used to determine a baseline susceptibly of cortex to 1M KCl induced spreading depression. A subsequent group of 5 WT and 5 KO animals was injected with 0.5 mg/kg LPS i.p. The CSD susceptibility was measured 72 hours later. The CSD number following the first KCl induced event was recorded for 1 hour. The results are shown in Figure 5 (* = WT vs WT(LPS) P <0.05; # = WT(LPS) vs. KO(LPS) P<0.05 One-way ANOVA Tukey's Multiple Comparison). LPS treatment reveals a GFAP cell expressing-STAT3 dependent reduction in CSD number in KO animals, an observation not seen in the untreated group (**Figure 19**). These data show that *the immunological activation associated with TBI has effects on cortical excitability.* It appears that LPS-induced immunological activation reduces cortical excitability, in a manner that is dependent on astrocytic STAT3 signaling pathway function. These results are being supplemented with histology and 2-photon imaging.

To ascertain the effect on cortical excitability of *hypotonic ACSF perfusion*, 10 animals were implanted acutely with microdialysis probes (PlasticsOne, 13 kD membrane, 1mm length, 1mm depth into cortex) through a 2 mm craniotomy centered between bregma, lambda, sagittal suture, and temporal ridge. ACSF (in mM: 125 NaCl, 3 KCl, 1.25 NaH2PO4, 2 CaCl2, 1 MgCl2, 25 NaHCO3, 11 glucose, pH 7.4) was perfused at 0.1 ml/hr, either at full strength, half dilution with distilled water, 2/3 dilution with distilled water, or 100% distilled water perfusion. Reflectance signal was collected from regions of interest between 100 - 200 µm of microdialysis probe, or > 1mm distant from probe. Next,

the same regions of interest were recorded during CSD. There was no significant difference in amplitude of either spontaneous or CSD-associated signal at any region of interest at any concentration of ACSF. Moreover, placement of microdialysis probes made analysis of signal closer to probe problematic. Finally, attempts at performing two-photon experiments with the microdialysis probe were unsuccessful because it was impossible to approximate the microscope objective to the tissue with the probe in place. We concluded that, due to the low yield of reflectance imaging and the impossibility of carrying out two-photon experiments even if reflectance imaging had been promising, that further microdialysis experiments should be deferred.

Task 1.e. Perform histological analysis on animals 24, 48, 72 hours, and 7 days after CCI TBI (Sofroniew, Brennan, Dudek, Months 1-24).

Histology using standard methods has been performed so far at the 48 hr and 7 days post injury time point. **Figure 20** shows the typical lesion pattern following our protocol. **Figure 21** shows Nissl stain at different magnifications including the CCI-lesioned region.

Figure 20: *Typical brain after PBS and PFA perfusion, the CCI injury is approximately 2 mm in diameter*.

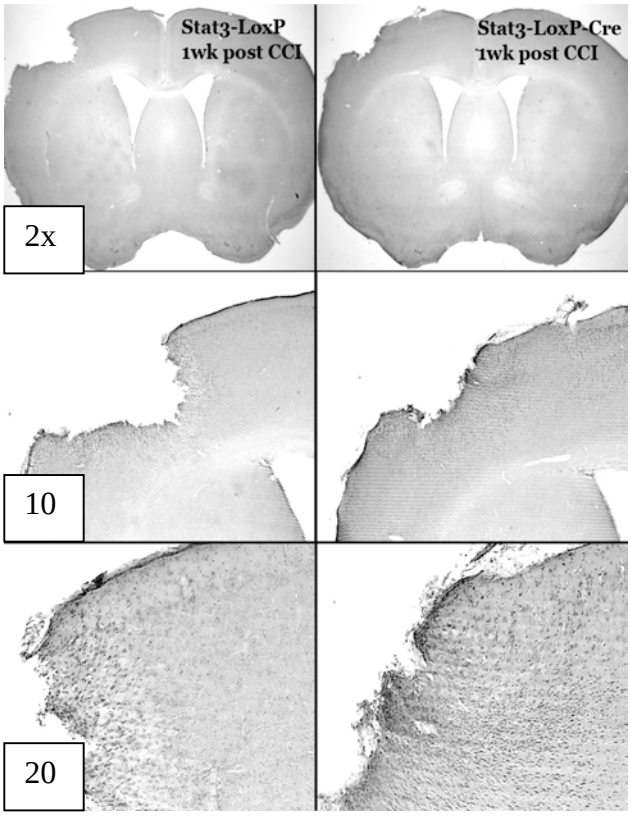

Figure 21. *Light microscopy images of Nissl stain displaying lesion area 1 week following impact in WT (Stat3-LoxP) and KO (Stat3-LoxP-Cre).*

Our full repertoire of antibodies has been successfully tested and is now being routinely used after TBI. **Figure 22** shows neuronal (NeuN), microglial (Iba1), and astrocytic (GFAP) in tissue from the same anatomic location ipsilateral and contralateral to CCI. Neuronal numbers are not appreciably changed past the location of the glial scar. However there is a significant increase in astrocyte as well as microglial cell body and process size in the peri-contusion region but not the contralateral hemisphere, consistent with both astrocytic and microglial activation reported after TBI.

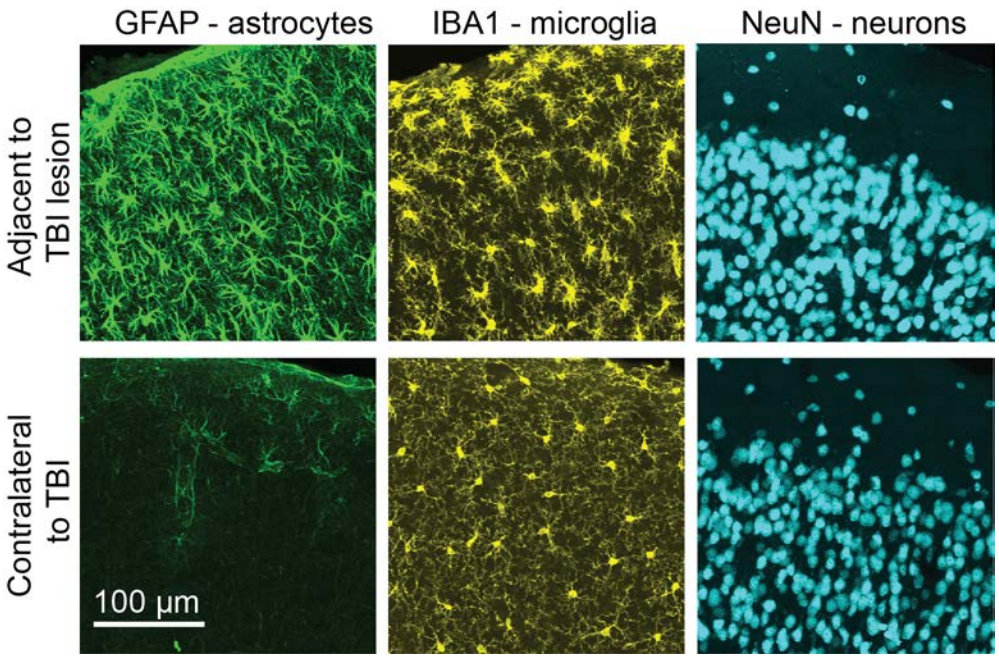

Figure 22: Tissue effects of TBI. *A. Cortical sections of wild-type animals, 48 h after CCI TBI. Top images show cortex ipsilateral to the site of TBI, immediately adjacent to the lesion. Bottom images show contralateral cortex. There is an ipsilateral increase in GFAP staining and change in astrocyte morphology compared to contralateral cortex, suggestive of astrogliosis near the site of injury. Similarly, ipsilateral microglia (labeled with IBA1) appear to have a different morphology compared to those in the contralateral cortex. There is a mild increase in NeuN staining (labels neuronal nuclei) intensity ipsilaterally, but no clear change in morphology or number. Images shown are maximum intensity projections of approx. 20 optical sections through a single cortical slice.*

Task 1.f. Perform plasma protein extravasation and brain water content experiments, analysis on animals 24, 48, 72 hours, 7 days after CCI TBI (Brennan/Dudek, Months 1-24).

Pending. These experiments are a subset of our histological analysis, however they require separate processing. We have delayed these experiments and advanced the other histological techiques we use (see above) as the other techniques can be performed together.

Task 1.g. Analyze results, correlate with histological and other experimental data, prepare data for publication (Brennan/Dudek, Sofroniew, Months 25-36).

Analysis shown for each task in context.

Task 2. Chronic experiments after CCI TBI (Brennan, Dudek, Months 1-36).

We are currently at month 18 of our grant (ACURO approval granted 6 months after 9/29/11 grant funding). Most of the experiments in task 2 begin at 24 months out. However, we have begun collecting data in earnest for several sub-tasks, and are collecting pilot data (e.g. for voltage sensitive dye imaging) for others. In addition, our preliminary data showing the effects of memantine on recovery from ischemic brain injury (relevant to Tasks 2.b. and 2.h.) have been submitted for publication, revised, and now resubmitted. The manuscript is attached as **Appendix 1**.

a. **Perform CCI, implant monitoring device, and monitor for chronic effects of TBI (3 months after injury)(Dudek, Months 18-24).**

Ongoing (see Task 1a above). So far 29 animals have had *continuous* monitoring out to 3 months after CCI. This is an improvement over our original protocol, which would have had monitoring only in a two-week window around the 3 month time point. This continuous monitoring offers the best chance of understanding the evolution of brain excitability changes after TBI. However it does have lower throughput. We are optimistic that we can complete the experiments but if need arises we can revert to the original protocol. Animals tested with either protocol will be comparable as their housing/recording conditions will have been identical.

b. **Perform CCI, implant monitoring device, and monitor for effects of memantine treatment after TBI (3 months after injury)(Dudek, Months 18-24).**

Pending completion of Task 2.a. above.

c. **Peform voltage sensitive dye experiments 3 months after CCI (Brennan, Months 24-36).**

Ongoing. We have performed 3 preliminary experiments so far to optimize VSDI acquisition in our new lab location.

d. **Perform CCI, two-photon experiments 3 months after CCI (Brennan, Dudek Months 24-36).**

Pending completion of acute two-photon experiments above.

e. **Perform histological analysis on animals 3 months after CCI TBI (Sofroniew, Brennan, Dudek, Months 18-36).**

Ongoing for all animals above.

f. **Perform plasma protein extravasation and brain water content experiments, analysis on animals 3 months after CCI TBI (Brennan/Dudek, Months 18-36).**

Pending. Will be performed simultaneous with task 1.f. above.

g. **Perform nociception behavior experiments (mechanical and thermal thresholds, rotarod) on animals 3 months after CCI TBI (Bates, Brennan, Months 18-36).**

Ongoing.

h. **Perform nociception behavior experiments (mechanical and thermal thresholds, rotarod) on animals 3 months after CCI TBI and treatment with memantine or placebo (Bates, Brennan, Months 18-36).**

Ongoing.

i. **Analyze results, correlate with histological and other experimental data, prepare data for publication (Brennan/Dudek, Bates, Sofroniew, months 25-36).**

Ongoing for each sub-task as task nears completion. Resubmission of preliminary data on recovery from ischemic injury with memantine.

KEY RESEARCH ACCOMPLISHMENTS

•Optimized controlled cortical impact TBI (CCI) parameters for mouse.

•Performing EEG monitoring of mice after CCI to monitor for seizures and cortical spreading depression (CSD), continuously out to 90 days after CCI.

•Implemented two-photon microscopy and whole cell recording *in vivo* after CCI; reportable outcomes.

•Measuring susceptibility to CSD after CCI, LPS, hypotonic ACSF; reportable outcomes.

•Measuring post-traumatic headache-relevant pain metrics after TBI.

•Optimization and implementation of majority of histological techniques.

REPORTABLE OUTCOMES

•Lipopolysaccharide (LPS) treatment, used to model inflammatory effects of TBI, reduces susceptibility CSD, but not in mice where astrocyte STAT3 signaling disrupted. To be supplemented by histology and 2-photon imaging.

•Altered sensory cortex pyramidal cell excitability phenotype after TBI. To be supplemented with additional experiments, possibly in vitro, to ascertain mechanism.

•Increased tissue displacement associated with CSD after TBI.

CONCLUSION

In the first eighteen months since the funding of this award we have established and validated all the experimental techniques we will need for the completion of the project, and have completed several datasets. We are now collecting publication-ready data for each sub-task and already have publication-ready data on TBI-associated immune activation, *in vivo* whole cell recording, and two-photon microscopy. Our next steps will be to complete acute experiments, and continue chronic experiments measuring long-term sequelae of TBI and their modulation with memantine. We are also attempting to extend our present work in order to maximize military-relevant synergies: we have applied for a second CDMRP award extending the present research; in doing so we continue to develop a collaboration with a University of Utah engineer (Dr. Kenneth Monson) performing blast TBI. Blast TBI is not part of this grant but enhances our ability to model all effects of military TBI. In addition, we have organized a Brain Injury Network involving alI TBI investigators at the University of Utah and the Wahlen VA. The goal of this group is to obtain a DOD or VA program grant application incorporating human and animal research.

So what?
If successful our work will:
•Define the natural history of excitable events in the brain after TBI.
•Determine the mechanisms of these excitable events.
•Develop treatments that prevent the progression to migraine and epilepsy after TBI.
If we achieve our goals, they will have a measurable impact on the quality of life of our service personnel, our veterans, and the civilian TBI population.

REFERENCES

1. Bruns, J. & Hauser, W. A. The Epidemiology of Traumatic Brain Injury: A Review. *Epilepsia* **44,** 2–10 (2003).
2. Ghajar, J. Traumatic brain injury. *Lancet* **356,** 923–929 (2000).
3. Rogawski, M. A. Common pathophysiologic mechanisms in migraine and epilepsy. *Arch. Neurol* **65,** 709–714 (2008).
4. D'Ambrosio, R. *et al.* Post-traumatic epilepsy following fluid percussion injury in the rat. *Brain* **127,** 304–314 (2004).
5. Cole, J. T. *et al.* Craniotomy: true sham for traumatic brain injury, or a sham of a sham? *J. Neurotrauma* **28,** 359–369 (2011).
6. Brody, D. L. *et al.* Electromagnetic controlled cortical impact device for precise, graded experimental traumatic brain injury. *J. Neurotrauma* **24,** 657–673 (2007).
7. Herrmann, J. E. *et al.* STAT3 is a critical regulator of astrogliosis and scar formation after spinal cord injury. *J. Neurosci* **28,** 7231–7243 (2008).
8. Aaronson, D. S. & Horvath, C. M. A road map for those who don't know JAK-STAT. *Science* **296,** 1653–1655 (2002).
9. Oliva, A. A., Jr, Kang, Y., Sanchez-Molano, J., Furones, C. & Atkins, C. M. STAT3 signaling after traumatic brain injury. *J. Neurochem.* **120,** 710–720 (2012).
10. Nimmerjahn, A., Kirchhoff, F., Kerr, J. N. D. & Helmchen, F. Sulforhodamine 101 as a specific marker of astroglia in the neocortex in vivo. *Nat Meth* **1,** 31–37 (2004).
11. Appaix, F. *et al.* Specific in vivo staining of astrocytes in the whole brain after intravenous injection of sulforhodamine dyes. *PLoS ONE* **7,** e35169 (2012).
12. Stosiek, C., Garaschuk, O., Holthoff, K. & Konnerth, A. In vivo two-photon calcium imaging of neuronal networks. *PNAS* **100,** 7319–7324 (2003).
13. Tian, L. *et al.* Imaging neural activity in worms, flies and mice with improved GCaMP calcium indicators. *Nat Meth* **6,** 875–881 (2009).
14. Zariwala, H. A. *et al.* A Cre-Dependent GCaMP3 Reporter Mouse for Neuronal Imaging In Vivo. *J. Neurosci.* **32,** 3131–3141 (2012).
15. Hirase, H., Qian, L., Barthó, P. & Buzsáki, G. Calcium Dynamics of Cortical Astrocytic Networks In Vivo. *PLoS Biol* **2,** e96 (2004).
16. Margrie, T., Brecht, M. & Sakmann, B. In vivo, low-resistance, whole-cell recordings from neurons in the anaesthetized and awake mammalian brain. *Pflügers Archiv European Journal of Physiology* **444,** 491–498 (2002).
17. Isaacson, J. S. & Scanziani, M. How inhibition shapes cortical activity. *Neuron* **72,** 231–243 (2011).
18. Kitamura, K., Judkewitz, B., Kano, M., Denk, W. & Häusser, M. Targeted patch-clamp recordings and single-cell electroporation of unlabeled neurons in vivo. *Nat. Methods* **5,** 61–67 (2008).
19. Brennan, K. C. *et al.* Casein kinase iδ mutations in familial migraine and advanced sleep phase. *Sci Transl Med* **5,** 183ra56, 1–11 (2013).
20. Lucas, S., Hoffman, J. M., Bell, K. R., Walker, W. & Dikmen, S. Characterization of headache after traumatic brain injury. *Cephalalgia* **32,** 600–606 (2012).
21. Kinlay, S. Changes in stroke epidemiology, prevention, and treatment. *Circulation* **124,** e494–496 (2011).
22. Roger, V. L. *et al.* Executive summary: heart disease and stroke statistics--2012 update: a report from the american heart association. *Circulation* **125,** 188–197 (2012).
23. Benowitz, L. I. & Carmichael, S. T. Promoting axonal rewiring to improve outcome after stroke. *Neurobiol. Dis.* **37,** 259–266 (2010).
24. Carmichael, S. T. Targets for neural repair therapies after stroke. *Stroke* **41,** S124–126 (2010).
25. Zhang, Z. G. & Chopp, M. Neurorestorative therapies for stroke: underlying mechanisms and translation to the clinic. *Lancet Neurol* **8,** 491–500 (2009).

26. Clarkson, A. N., Huang, B. S., Macisaac, S. E., Mody, I. & Carmichael, S. T. Reducing excessive GABA-mediated tonic inhibition promotes functional recovery after stroke. *Nature* **468,** 305–309 (2010).
27. Clarkson, A. N. *et al.* AMPA receptor-induced local brain-derived neurotrophic factor signaling mediates motor recovery after stroke. *J. Neurosci.* **31,** 3766–3775 (2011).
28. Rammes, G., Danysz, W. & Parsons, C. G. Pharmacodynamics of memantine: an update. *Curr Neuropharmacol* **6,** 55–78 (2008).
29. Thomas, S. J. & Grossberg, G. T. Memantine: a review of studies into its safety and efficacy in treating Alzheimer's disease and other dementias. *Clin Interv Aging* **4,** 367–377 (2009).
30. Marvanová, M. *et al.* The neuroprotective agent memantine induces brain-derived neurotrophic factor and trkB receptor expression in rat brain. *Mol. Cell. Neurosci.* **18,** 247–258 (2001).
31. Meisner, F. *et al.* Memantine upregulates BDNF and prevents dopamine deficits in SIV-infected macaques: a novel pharmacological action of memantine. *Neuropsychopharmacology* **33,** 2228–2236 (2008).
32. Murphy, T. H. & Corbett, D. Plasticity during stroke recovery: from synapse to behaviour. *Nat. Rev. Neurosci.* **10,** 861–872 (2009).
33. Minkeviciene, R., Banerjee, P. & Tanila, H. Memantine improves spatial learning in a transgenic mouse model of Alzheimer's disease. *J. Pharmacol. Exp. Ther* **311,** 677–682 (2004).
34. Kornhuber, J. & Quack, G. Cerebrospinal fluid and serum concentrations of the N-methyl-D-aspartate (NMDA) receptor antagonist memantine in man. *Neurosci. Lett.* **195,** 137–139 (1995).
35. Grinvald, A., Lieke, E., Frostig, R. D., Gilbert, C. D. & Wiesel, T. N. Functional architecture of cortex revealed by optical imaging of intrinsic signals. *Nature* **324,** 361–4 (1986).
36. Frostig, R. D., Lieke, E. E., Ts'o, D. Y. & Grinvald, A. Cortical functional architecture and local coupling between neuronal activity and the microcirculation revealed by in vivo high-resolution optical imaging of intrinsic signals. *Proc Natl Acad Sci U S A* **87,** 6082–6086 (1990).
37. Franklin, K. & Paxinos, G. *The Mouse Brain in Stereotaxic Coordinates.* (Academic Press, 1997).
38. Rasband, W. S. ImageJ, US National Institutes of Health, Bethesda, Maryland, USA. (1997). at <http://imagej.nih.gov/ij/>
39. Schallert, T., Fleming, S. M., Leasure, J. L., Tillerson, J. L. & Bland, S. T. CNS plasticity and assessment of forelimb sensorimotor outcome in unilateral rat models of stroke, cortical ablation, parkinsonism and spinal cord injury. *Neuropharmacology* **39,** 777–787 (2000).
40. Li, X. *et al.* Chronic behavioral testing after focal ischemia in the mouse: functional recovery and the effects of gender. *Exp. Neurol.* **187,** 94–104 (2004).
41. Kleim, J. A., Boychuk, J. A. & Adkins, D. L. Rat models of upper extremity impairment in stroke. *ILAR J* **48,** 374–384 (2007).
42. Martinez-Coria, H. *et al.* Memantine improves cognition and reduces Alzheimer's-like neuropathology in transgenic mice. *Am. J. Pathol.* **176,** 870–880 (2010).
43. Ohab, J. J., Fleming, S., Blesch, A. & Carmichael, S. T. A neurovascular niche for neurogenesis after stroke. *J. Neurosci.* **26,** 13007–13016 (2006).
44. Myer, D. J., Gurkoff, G. G., Lee, S. M., Hovda, D. A. & Sofroniew, M. V. Essential protective roles of reactive astrocytes in traumatic brain injury. *Brain* **129,** 2761–2772 (2006).
45. Lapchak, P. A. Memantine, an uncompetitive low affinity NMDA open-channel antagonist improves clinical rating scores in a multiple infarct embolic stroke model in rabbits. *Brain Res.* **1088,** 141–147 (2006).
46. Babu, C. S. & Ramanathan, M. Pre-ischemic treatment with memantine reversed the neurochemical and behavioural parameters but not energy metabolites in middle cerebral artery occluded rats. *Pharmacol. Biochem. Behav.* **92,** 424–432 (2009).
47. Sofroniew, M. V. Molecular dissection of reactive astrogliosis and glial scar formation. *Trends Neurosci* **32,** 638–647 (2009).
48. Ploughman, M. *et al.* Brain-derived neurotrophic factor contributes to recovery of skilled reaching after focal ischemia in rats. *Stroke* **40,** 1490–1495 (2009).

49. Ke, Z., Yip, S. P., Li, L., Zheng, X.-X. & Tong, K.-Y. The effects of voluntary, involuntary, and forced exercises on brain-derived neurotrophic factor and motor function recovery: a rat brain ischemia model. *PLoS ONE* **6,** e16643 (2011).
50. Chen *et al.* Neuroprotective concentrations of the N-methyl-D-aspartate open-channel blocker memantine are effective without cytoplasmic vacuolation following post-ischemic administration and do not block maze learning or long-term potentiation. *Neuroscience* **86,** 1121–1132 (1998).
51. Görgülü, A. *et al.* Reduction of edema and infarction by Memantine and MK-801 after focal cerebral ischaemia and reperfusion in rat. *Acta Neurochir (Wien)* **142,** 1287–1292 (2000).
52. Brown, C. E., Li, P., Boyd, J. D., Delaney, K. R. & Murphy, T. H. Extensive turnover of dendritic spines and vascular remodeling in cortical tissues recovering from stroke. *J. Neurosci.* **27,** 4101–4109 (2007).
53. Chen, H.-S. V. & Lipton, S. A. The chemical biology of clinically tolerated NMDA receptor antagonists. *J. Neurochem* **97,** 1611–1626 (2006).
54. Johnson, J. W. & Kotermanski, S. E. Mechanism of action of memantine. *Curr Opin Pharmacol* **6,** 61–67 (2006).
55. David-Jürgens, M., Churs, L., Berkefeld, T., Zepka, R. F. & Dinse, H. R. Differential effects of aging on fore- and hindpaw maps of rat somatosensory cortex. *PLoS ONE* **3,** e3399 (2008).
56. Brown, C. E., Aminoltejari, K., Erb, H., Winship, I. R. & Murphy, T. H. In vivo voltage-sensitive dye imaging in adult mice reveals that somatosensory maps lost to stroke are replaced over weeks by new structural and functional circuits with prolonged modes of activation within both the peri-infarct zone and distant sites. *J. Neurosci* **29,** 1719–1734 (2009).
57. Klein, A., Sacrey, L.-A. R., Whishaw, I. Q. & Dunnett, S. B. The use of rodent skilled reaching as a translational model for investigating brain damage and disease. *Neurosci Biobehav Rev* **36,** 1030–1042 (2012).
58. Ramanathan, D., Conner, J. M. & Tuszynski, M. H. A form of motor cortical plasticity that correlates with recovery of function after brain injury. *Proc. Natl. Acad. Sci. U.S.A.* **103,** 11370–11375 (2006).
59. Jones, T. A. *et al.* Remodeling the Brain With Behavioral Experience After Stroke. *Stroke* **40,** S136–S138 (2009).
60. Li, S. *et al.* An age-related sprouting transcriptome provides molecular control of axonal sprouting after stroke. *Nat. Neurosci* **13,** 1496–1504 (2010).
61. Matyas, F. *et al.* Motor control by sensory cortex. *Science* **330,** 1240–1243 (2010).
62. Kermani, P. & Hempstead, B. Brain-derived neurotrophic factor: a newly described mediator of angiogenesis. *Trends Cardiovasc. Med.* **17,** 140–143 (2007).
63. Leventhal, C., Rafii, S., Rafii, D., Shahar, A. & Goldman, S. A. Endothelial trophic support of neuronal production and recruitment from the adult mammalian subependyma. *Mol. Cell. Neurosci.* **13,** 450–464 (1999).
64. Qin, L., Kim, E., Ratan, R., Lee, F. S. & Cho, S. Genetic variant of BDNF (Val66Met) polymorphism attenuates stroke-induced angiogenic responses by enhancing anti-angiogenic mediator CD36 expression. *J. Neurosci.* **31,** 775–783 (2011).
65. Prakash, Cohen-Cory, S. & Frostig, R. D. Rapid and opposite effects of BDNF and NGF on the functional organization of the adult cortex in vivo. *Nature* **381,** 702–706 (1996).
66. Li, Y. *et al.* Gliosis and brain remodeling after treatment of stroke in rats with marrow stromal cells. *Glia* **49,** 407–417 (2005).
67. Bacigaluppi, M. *et al.* Delayed post-ischaemic neuroprotection following systemic neural stem cell transplantation involves multiple mechanisms. *Brain* **132,** 2239–2251 (2009).
68. Xia, P., Chen, H. V., Zhang, D. & Lipton, S. A. Memantine preferentially blocks extrasynaptic over synaptic NMDA receptor currents in hippocampal autapses. *J. Neurosci.* **30,** 11246–11250 (2010).
69. Hardingham, G. E. & Bading, H. Synaptic versus extrasynaptic NMDA receptor signalling: implications for neurodegenerative disorders. *Nat. Rev. Neurosci.* **11,** 682–696 (2010).

70. Peeters, M. *et al.* Effects of pan- and subtype-selective NMDA receptor antagonists on cortical spreading depression in the rat: therapeutic potential for migraine. *J Pharmacol Exp Ther* **321,** 564–72 (2007).
71. Sukhotinsky, I. *et al.* Chronic daily cortical spreading depressions suppress spreading depression susceptibility. *Cephalalgia* **31,** 1601–1608 (2011).
72. Lauritzen, M. *et al.* Clinical relevance of cortical spreading depression in neurological disorders: migraine, malignant stroke, subarachnoid and intracranial hemorrhage, and traumatic brain injury. *J. Cereb. Blood Flow Metab.* **31,** 17–35 (2011).
73. Schinder, A. F. & Poo, M. The neurotrophin hypothesis for synaptic plasticity. *Trends Neurosci.* **23,** 639–645 (2000).
74. Nagappan, G. & Lu, B. Activity-dependent modulation of the BDNF receptor TrkB: mechanisms and implications. *Trends Neurosci.* **28,** 464–471 (2005).
75. Sulejczak, D. *et al.* Focal photothrombotic lesion of the rat motor cortex increases BDNF levels in motor-sensory cortical areas not accompanied by recovery of forelimb motor skills. *J. Neurotrauma* **24,** 1362–1377 (2007).
76. Chen, J. *et al.* Endothelial nitric oxide synthase regulates brain-derived neurotrophic factor expression and neurogenesis after stroke in mice. *J. Neurosci.* **25,** 2366–2375 (2005).
77. Molinaro, G. *et al.* Memantine treatment reduces the expression of the K(+)/Cl(-) cotransporter KCC2 in the hippocampus and cerebral cortex, and attenuates behavioural responses mediated by GABA(A) receptor activation in mice. *Brain Res.* **1265,** 75–79 (2009).
78. Al-Amin, H., Sarkis, R., Atweh, S., Jabbur, S. & Saadé, N. Chronic dizocilpine or apomorphine and development of neuropathy in two animal models II: effects on brain cytokines and neurotrophins. *Exp. Neurol.* **228,** 30–40 (2011).
79. Guo, C., Yang, Y., Su, Y. & Si, T. Postnatal BDNF expression profiles in prefrontal cortex and hippocampus of a rat schizophrenia model induced by MK-801 administration. *J. Biomed. Biotechnol.* **2010,** 783297 (2010).
80. Marvanová, M., Lakso, M. & Wong, G. Identification of genes regulated by memantine and MK-801 in adult rat brain by cDNA microarray analysis. *Neuropsychopharmacology* **29,** 1070–1079 (2004).
81. Baumbauer, K. M., Huie, J. R., Hughes, A. J. & Grau, J. W. Timing in the absence of supraspinal input II: regularly spaced stimulation induces a lasting alteration in spinal function that depends on the NMDA receptor, BDNF release, and protein synthesis. *J. Neurosci.* **29,** 14383–14393 (2009).
82. Ninan, I. *et al.* The BDNF Val66Met polymorphism impairs NMDA receptor-dependent synaptic plasticity in the hippocampus. *J. Neurosci.* **30,** 8866–8870 (2010).
83. Chen, L. Y., Rex, C. S., Pham, D. T., Lynch, G. & Gall, C. M. BDNF signaling during learning is regionally differentiated within hippocampus. *J. Neurosci.* **30,** 15097–15101 (2010).
84. Dietrich, W. D. *et al.* Thromboembolic events lead to cortical spreading depression and expression of c-fos, brain-derived neurotrophic factor, glial fibrillary acidic protein, and heat shock protein 70 mRNA in rats. *J. Cereb. Blood Flow Metab.* **20,** 103–111 (2000).
85. Berthier, M. L. *et al.* Memantine and constraint-induced aphasia therapy in chronic poststroke aphasia. *Ann. Neurol.* **65,** 577–585 (2009).

APPENDICES

Appendix 1: Submitted Manuscript: *Memantine enhances recovery from stroke.*

Memantine enhances recovery from stroke.

Running title: Memantine in stroke recovery.

Héctor E. López-Valdés1*, Andrew N. Clarkson1,2*, Yan Ao3, S. Thomas Carmichael1 , Michael V. Sofroniew3, and K.C. Brennan1,4**

1. Department of Neurology, David Geffen School of Medicine at UCLA, 90095.

2. Departments of Anatomy and Psychology, University of Otago, NZ, 9054.

3. Department of Neurobiology, David Geffen School of Medicine at UCLA, 90095.

4. Present Address: Department of Neurology, University of Utah School of Medicine

*These authors contributed equally to this work.

**To whom correspondence should be addressed.

383 Colorow Drive, Room 364, Salt Lake City UT 84103.

k.c.brennan@hsc.utah.edu.

Number of pages: 37; Number of figures: 7; Number of words: Abstract 203; Introduction 288, Discussion 1090.

Conflict of Interest: The authors declare no competing financial interests.

Acknowledgements: This work was supported by the Larry L. Hillblom Foundation (HLV, STC); an American Heart Association Postdoctoral Fellowship, a Repatriation Fellowship from the New Zealand Neurological Foundation and the Sir Charles Hercus Fellowship from the Health Research Council of New Zealand (ANC); and the National Institutes of Health NS053957 (STC), NS057624 (MVS); NS059072 and NS070084 (KCB).

Abstract

Stroke treatment is constrained by extremely limited treatment windows, and the clinical inefficacy of agents that showed preclinical promise. Yet animal and clinical data suggest considerable post-stroke plasticity, which could allow for treatment with recovery-modulating agents. Memantine (MEM) is a well-tolerated N-methyl D-aspartate (NMDA) glutamate receptor antagonist in common use for Alzheimer's disease. MEM, 30mg/kg/day, or vehicle, was delivered chronically in drinking water beginning more than 2 hours after photothrombotic stroke. No difference in infarct size or neuronal number was noted, showing that no neuroprotective effects were present. However, mice treated chronically with MEM showed significant improvements in motor control as measured by cylinder test and grid walking performance compared to vehicle treated animals. Optical intrinsic signal (OIS) imaging revealed an increased area of forepaw sensory maps. There was decreased reactive astrogliosis and increased vascular density around the infarcted cortex. Peri-infarct Western blots revealed increased brain-derived neurotrophic factor (BDNF) and phosphorylated-Tropomyosin-related kinase B receptor (p-TrkB) expression. Our results suggest that MEM improves stroke outcome in a non-neuroprotective manner involving increased BDNF signaling, reduced reactive astrogliosis and improved vascularization, associated with improved recovery of sensory and motor cortical function. The clinical availability and tolerability of MEM make it an attractive candidate for clinical translation.

Introduction

Stroke is the fourth leading cause of death, and is a major cause of morbidity worldwide (Kinlay, 2011; Roger et al., 2012). Despite an enormous amount of research, treatment options are limited. Tissue plasminogen activator (the only FDA-approved treatment for stroke) is restricted in its use to the few hours after stroke, and beyond this narrow time window treatment is limited to supportive care, secondary prevention, and rehabilitation techniques (Zhang and Chopp, 2009; Benowitz and Carmichael, 2010; Carmichael, 2010). Neuroprotection, the prevention of cell death beyond the boundaries of the infarct core, has been disappointing in translation from animal models to human studies. Despite the loss of neuronal tissue, considerable plasticity is retained after stroke in both animal models and in humans. The manipulation of the recovery process has emerged as an alternative and potentially more tractable target in stroke research (Zhang and Chopp, 2009; Clarkson et al., 2010, 2011).

Memantine (MEM) is a non-competitive, use-dependent NMDA antagonist, which is used to treat Alzheimer's disease (Rammes et al., 2008; Thomas and Grossberg, 2009). As an NMDA antagonist, MEM has been tested for neuroprotective effects and reduces infarct size when given acutely (Chen et al., 1998; Görgülü et al., 2000; Lapchak, 2006; Hao et al., 2008; Babu and Ramanathan, 2009; Liu et al., 2009; Shih et al., 2013). However, MEM has other effects that may be relevant beyond the acute setting. For example, MEM treatment causes an increase in secretion of brain-derived neurotrophic factor (BDNF) (Marvanová et al., 2001; Meisner et al., 2008), which is involved in cortical plasticity after stroke (Murphy and Corbett, 2009; Clarkson et al., 2011).

We treated mice chronically with MEM or vehicle, using doses specifically designed to mimic those that produced usual serum concentrations in humans (Minkeviciene et al., 2004), delivered so as to avoid neuroprotective effects. We found that despite an absence of neuroprotection, MEM improved stroke outcome as measured by behavioral testing and recovery of functional sensory maps. This effect was associated with decreased reactive astrogliosis, increased vascular density, and increased BDNF and p-TrkB expression. Given

the tolerability of MEM in an aged population with characteristics similar to stroke patients, our results may have direct translational relevance.

Materials and Methods

Induction of Focal Ischemia

All protocols were approved by the Animal Research Committee of the University of California. Male C57BL/6J mice (n=66; 28-32g) were anesthetized with isoflurane and placed in a stereotactic frame in a sterile field, where a midline scalp incision exposed the skull overlying the left motor and somatosensory cortex. A cold light source attached to a 40× objective and giving a 2-mm diameter circle of illumination was positioned 1.5mm lateral from Bregma. Rose Bengal (200μl of a 10mg/ml solution; Sigma) was injected intraperitoneally 5 minutes prior to induction of photothrombosis, which was induced with fifteen minutes of irradiation (Clarkson et al., 2010, 2013). At the end of the experiment, the scalp was cleaned with sterile saline solution and sutured, and the animals were allowed to recover.

Sensory mapping

Optical intrinsic signal imaging (OIS) was performed 7 days before and 7, 14, 21 and 28 days after focal ischemia, as described (Clarkson et al., 2013). Briefly, mice were anesthetized with enflurane (4% induction, 1.5- 2% maintenance), the skull was exposed, and coated with silicone oil for transparency. For anatomical reference, the cortical surface vessels of the left hemisphere were recorded through the intact skull using green illumination. After that, the field of view was defocused 300-350 μm below the vessels, and the illumination was changed to red for recording of sensory maps. Electrical stimulation (50Hz, 0.001s pulse width, 0.14-0.22 mA) was delivered to the forepaw and hindpaw (FP, HP) through pairs of subdermal needle electrodes, beginning 5s after the start of each trial; trial duration was 25s. An image session consisted of 32 trials for each FP and HP, with an intertrial interval of 5s, alternating between FP and HP. Image acquisition and electric stimulation were controlled with a custom LabView virtual instrument.

Memantine Treatment

Mice were randomly assigned to treatment for 28 days with memantine (1-amino-3,5-dimethyl-adamantane; Sigma) HCL (30 mg/kg/day in a 2% sucrose solution (Minkeviciene et al., 2004)) or 2% sucrose vehicle

delivered continuously in drinking water, beginning 2 hours after photothrombosis. This dosing regimen results in serum concentrations of ~1μM in C57Bl/6J mice, comparable to the therapeutic plasma concentration in humans (Kornhuber and Quack, 1995; Minkeviciene et al., 2004).

Data Processing and Analysis.

Normalized images (ΔR/R; normalized to averaged prestimulus frames) were filtered (3-pixel half-width Gaussian) to remove high frequency noise. Functional response area was quantified as the area whose pixels showed a stimulus response greater than 50% of maximum response. Image analysis was performed using either plugins or custom routines written for ImageJ 1.40g (Rasband, 1997).

Behavioral testing and analysis

Cylinder test and grid-walking test were performed 7 days before, and 7, 14, 21, and 28 days after stroke (**Figure 1A**). *Cylinder test.* Animals were placed in a clear acrylic cylinder and were videotaped for 10 min in order to determine forelimb preference. Video footage was analyzed offline by raters blinded to treatment group. The total number of cylinder contacts with left, right and both forelimbs were counted and the index for preference was obtained following the formula: Index=(Left–Right)/(Left+Right+simultaneous) (Schallert et al., 2000; Li et al., 2004; Kleim et al., 2007). *Grid-walking test* was carried out as previously described(Clarkson et al., 2010, 2011). Each mouse was placed individually atop an elevated wire grid and allowed to freely walk for a period of 5min. Video footage was analyzed offline by binded raters. The total number of foot-faults for each limb, along with the total number of non-foot-fault steps, was counted, and a ratio between foot-faults and total-steps-taken calculated.

Protein extraction and Western blot analysis

Mice were sacrificed by overdose of halothane and rapidly decapitated. Brains were placed in a mouse matrix in which a 2 mm coronal section was cut , -1 mm to +1 mm from bregma. This section included the whole ischemic area (left hemisphere) and cognate regions from the contralateral uninjured hemisphere (**Figure 1B**). The tissue section was cut sagittally along the midline and both hemispheres were separately frozen in dry ice for biochemical analysis. Protein extracts were prepared by homogenizing whole brain hemisphere samples in extraction buffer complemented with a protease and phosphatase inhibitors, followed by centrifugation at 100,000 x *g* for 1 hour. Protein concentration in the supernatant was determined using the Bradford assay. Equal amounts of protein per sample were loaded in 4 to 12% gradient gels and transferred to nitrocellulose membranes. Membranes were blocked for 1 hour in 5% (v/v) suspension of nonfat milk or bovine serum albumin in 0.2% Tween-20 Tris-buffered saline (pH 7.5), and processed as described(Martinez-Coria et al., 2010 p.-). Primary antibodies used for Western blots were anti-VEGF (1:1000, Millipore), anti-GDNF, (1:1000, Abcam), anti-BDNF (1:1000, Abcam), anti-Trk-B (1:1000, Abcam), anti-phospho-Trk-B (1:500, Abcam). Quantitative densiometric analyses were performed using the Gel Analyzer Plugin for ImageJ 1.40g.

Histology

Mice were sacrificed by overdose of halothane, and perfused transcardially with 0.9 % NaCl followed by 4% paraformaldehyde in phosphate-buffered saline, pH 7.4, 7 or 28 days after photothrombosis. Brains were removed, post-fixed for 2 hours and cryoprotected in 30% sucrose overnight. Forty-µm frozen sections were cut with a cryostat (Leica, Nussloch, Germany) and stored in cryoprotectant solution pending further processing. Every third section was collected to quantify infarct volumes using cresyl violet (Nissl) stain (Ohab et al., 2006; Clarkson et al., 2010). Because no differences were detected between the patterns of staining in the cerebral cortex of intact animals and those found in cortex contralateral to the infarcted hemisphere in operated animals, in each subject the contralateral hemicortex served as control. Immunohistochemical staining of glial fibrillary acidic protein (GFAP), neuronal nuclear antigen (NeuN) and platelet endothelial cell adhesion molecule (PECAM-1) were used to evaluate gliosis, neuronal and blood vessel density, respectively. Brightfield immunohistochemistry was performed using biotinylated secondary antibodies (Vector, Burlingame, CA),

biotin-avidin-peroxidase complex (Vector) and diaminobenzidine (DAB, Vector) as the developing agent as described (Myer et al., 2006). Primary antibodies were: rabbit anti-GFAP (1:10,000; Dako), rat ant-PECAM-1 (1:400; BD-Pharmigen), bio-NeuN (1:2500; Millipore). Stained sections were examined and photographed using brightfield microscopy. Image analysis was conducted using ImageJ 1.40g. Immunohistochemical images from animals with stroke were analyzed from the border of the glial scar to a lateral distance of 2100 μm, divided into 6 regions (350 μm width, **Figures 2, 5, 6**). Sham treated animals were analyzed over identical cortical regions. Because post-stroke scarring causes changes in cortical thickness, all measures were normalized to the area of the region analyzed.

Statistical Analysis.

All experiments were performed in accordance with ARRIVE and NINDS guidelines (Kilkenny et al., 2010; Landis et al., 2012). Group sizes were determined from our previous work in similar models (Clarkson et al., 2010, 2011, 2013). Animals were randomized to treatment vs. sham groups, and experimenters and raters were blinded to group identity. Comparisons were made with ANOVA methods with post-hoc testing, after verification that data were appropriate for parametric testing. A p value <0.05 was considered statistically significant. Data are expressed as the mean ± SEM.

Results

Identical infarct size and neuronal density in MEM- and vehicle-treated animals.

Consistent with previous work (Clarkson et al., 2010, 2013) an infarct centered 1.5mm lateral to Bregma affected primary motor cortex as well as FP and HP sensory cortex (Tennant et al., 2011), with HP sensory cortex being more severely affected (**Figure 2A,B**). There was no difference in infarct size measured by Nissl staining between MEM- and vehicle-treated animals (**Figure 2A-C**), consistent with other work in which MEM was given more than 2 hours after ischemia (Lapchak, 2006; Babu and Ramanathan, 2009). NeuN staining was used to measure neuronal density and cell size in the peri-infarct region, and showed no difference between treated and untreated animals (**Figure 2D-H**). We concluded that MEM was not exerting neuroprotective effects using our treatment regimen.

Improved forepaw behavioral recovery in MEM-treated animals.

Despite identical infarct volumes, there was significant improvement in behavioral measures of recovery in MEM-treated mice compared to vehicle-treated animals. The cylinder test measures exploratory forelimb movements, and is used to measure functional recovery from stroke (Kleim et al., 2007; Clarkson et al., 2010, 2011). Though both MEM- and vehicle-treated animals showed a significant increase in forelimb use asymmetry after stroke, MEM-treated animals showed a progressive recovery of the impaired limb, which was significant at 28 days post-stroke (**Figure 3A**). The grid-walking test is another measure of post-stroke functional recovery (Clarkson et al., 2010, 2011) which measures both fore- and hindlimb function. There was a significant increase in FP and HP foot faults after stroke and a subsequent slow recovery of function. MEM-treated animals showed a greater reduction in FP (but not HP) foot-faults, which became significant 28 days after stroke (**Figure 3B,C**). The combined behavioral test data indicates that MEM treatment was associated with improved functional recovery of FP, but not HP, function after stroke.

Improved functional recovery of forepaw sensory maps with MEM treatment.

We used OIS to measure FP and HP sensory maps before and after stroke as a measure of the physiology of the peri-infarct cortex during recovery. FP and HP stimulation produced distinct regions of activation in primary somatosensory cortex (**Figure 4A**), which were essentially abolished after stroke. FP maps showed a significant increase in cortical activation area in MEM-treated compared to vehicle-treated animals at 28 days after stroke. The area of activation for both FP and HP sensory maps slowly increased during stroke recovery, but remained substantially below pre-stroke conditions for all animals, whether treated with MEM or not (**Figure 4B,C**). There was no significant difference in area of activation of HP maps with MEM treatment, and neither the increases in FP or HP maps for vehicle treated animals were significant. Our functional activation data thus showed a similar pattern to behavioral data, with improved recovery in FP but not HP function with MEM treatment.

Decreased reactive astrogliosis and increased vascular density in peri-infarct cortex of MEM-treated animals.

Stroke centered over forepaw motor cortex resulted in a consistent, full-cortical-thickness lesion, which at 28 days consisted of a core region of necrotic tissue ($1.13\pm0.12mm^3$ stroke+vehicle; $1.22\pm0.10mm^3$ stroke+MEM). As expected in control animals, this lesion was encircled by an immediate border of mature, compact glial scar and a surrounding zone of moderate to mild reactive astrogliosis (Sofroniew, 2009) that exhibited a gradient of elevated GFAP expression that was highest near the lesion and declined until it became indistinguishable from that of the control hemisphere at distances greater than 1770 μm from the lesion border (**Figure 5B,C**). Vascular density, measured by PECAM1 staining of the endothelium, was maximally decreased in the immediate vicinity of the infarct lesion and exhibited a gradient of improvement, becoming indistinguishable from control hemisphere at distances greater than 2mm from the lesion border (**Figure 6B,C**). In MEM-treated animals, these gradients of changes in GFAP and PECAM1 immunoreactivity were significantly altered. The total area of GFAP expressing cells was significantly reduced in MEM-treated compared to vehicle-treated animals in each region of interest at increasing distances from the lesion border. GFAP expression in MEM-treated animals became indistinguishable from control hemisphere beginning 750μm from the lesion border

(**Figure 5D**). PECAM1 expression density was significantly *increased* in MEM-treated vs. vehicle treated animals within the first three zones of tissue (0-750μm) adjacent to the lesion border (**Figure 6D,E**).

Increased BDNF pathway signaling in peri-infarct cortex of MEM-treated animals.

BDNF expression is increased during stroke recovery (Ploughman et al., 2009; Clarkson et al., 2011; Ke et al., 2011), and our findings of alterations in glial reactivity and vascular morphology motivated an examination of GDNF and VEGF. We found no difference in GDNF or VEGF expression by Western blot, in peri-infarct cortex. However, there was a significant increase in BDNF expression in MEM- compared to vehicle-treated animals in peri-infarct cortex during the period of stroke recovery. Consistent with this increase in expression, p-TrkB expression was also increased in this region (**Figure 7**).

Discussion

We have shown that chronic treatment with a clinically tolerated medication, dosed to deliver concentrations comparable to human use, improves stroke outcome. The improvements occurred despite the fact that MEM was delivered orally *after* the stroke, and the fact that neuroprotection was not observed. The translational significance of this finding is two-fold. Firstly, it suggests a treatment for stroke recovery that is clinically feasible. Secondly, it suggests that stroke recovery can be improved without the stringent time-dependency of neuroprotective strategies.

Recovery-promoting vs. neuroprotective effects of orally-dosed MEM.

MEM is an NMDA antagonist and is neuroprotective when given before (Babu and Ramanathan, 2009), and sometimes within the first two hours after stroke (Chen et al., 1998; Görgülü et al., 2000; Lapchak, 2006; Babu and Ramanathan, 2009; Shih et al., 2013). In contrast, we observed no evidence of neuroprotection. Studies showing neuroprotection all used intraperitoneal dosing less than 2 hours after stroke, whereas we delivered MEM in drinking water later after the event. This may account for the lack of neuroprotection we observed. Whatever the mechanism, the lack of neuroprotection is important, as it allows us to specifically assess the effects on post-stroke recovery.

Improved sensorimotor recovery in MEM-treated animals.

Cylinder and grid walking tests document stroke recovery (Clarkson et al., 2010, 2011) and OIS imaging has been used to demonstrate sensory map plasticity after stroke (Brown et al., 2007; Clarkson et al., 2013). We used both behavioral and physiological measures of sensorimotor cortex function to determine the effects of MEM on stroke recovery.

We observed improvements in both behavior and OIS imaging following MEM compared to vehicle treatment. Interestingly, both tests showed improvement in FP, but not HP, behavior and sensory maps. This is likely due to greater destruction of HP cortex by our stroke technique (**Figures 1,2**). However other explanations might be

considered. MEM is an activity-dependent blocker of NMDA receptors(Chen and Lipton, 2006; Johnson and Kotermanski, 2006): The differential use of the FP compared to HP (e.g. for exploratory activity) might account for a greater effect on FP sensory maps and behavioral function than HP. There are also intrinsic differences in FP and HP excitability and plasticity in rodents which might explain a difference in post-stroke recovery between the two cortices (David-Jürgens et al., 2008; Brown et al., 2009).

Because cylinder test and grid-walking examine both sensory and motor function, and because our infarct region affected both sensory and motor cortex, it is not possible to distinguish sensory and motor recovery mechanisms with precision. FP and HP sensory map testing is specific to sensory function, and confirms differential map plasticity in MEM-treated animals after stroke, but it is very likely that motor plasticity also occurred because of its prominent role in stroke recovery (Ramanathan et al., 2006; Jones et al., 2009). There are also extensive reciprocal connections between sensory and motor cortices, arguing that plasticity in one region would likely be accompanied by plasticity in the other. Such changes could be associated with sprouting of new connections (Li et al., 2010), synaptogenesis (Clarkson et al., 2011) or unmasking of quiescent connections (Clarkson et al., 2010), among several mechanisms.

Increased vascular density.

OIS maps are generated primarily by increases in blood volume or oxygenation, specific to the activated region of cortex (Grinvald et al., 1986; Frostig et al., 1990), and functional stroke recovery is correlated with recovery of vascular density in peri-infarct regions (Zhang and Chopp, 2009). We found that PECAM1 staining, which outlines vascular endothelium, was increased within 0-750 μm of tissue adjacent to the lesion border in MEM-treated compared to vehicle-treated animals. This area corresponds to regions activated on OIS mapping (**Figures 1, 4**). Vascular integrity is a prerequisite for survival of peri-infarct tissue and subsequent functional recovery, and during stroke recovery, vascular and neural plasticity are linked (Ohab et al., 2006; Zhang and Chopp, 2009). It is thus likely that OIS map plasticity and behavioral recovery were mutually dependent processes in MEM-treated animals. How those changes were driven is less clear. The lack of a significant

difference in VEGF between MEM- and vehicle-treated animals argues against this pathway. However BDNF signaling has been shown to be involved in angiogenesis (Kermani and Hempstead, 2007), and BDNF polymorphisms, associated with poor stroke outcome in humans, show reduced angiogenesis in animal models (Qin et al., 2011).

Decreased GFAP expression.

GFAP expression is a hallmark of reactive astrogliosis (Sofroniew, 2009). Our observation of a decrease in GFAP immunoreactivity in peri-infarct cortex after MEM-treatment is consistent with other reports associating improved stroke recovery with reduced astrocytic reactivity (Li et al., 2005; Bacigaluppi et al., 2009). The cause of the reduced GFAP expression after MEM-treatment in our animals has several potential explanations. MEM treatment could have reduced extrasynaptic glutamate signaling (Hardingham and Bading, 2010; Xia et al., 2010) which in turn reduced the production of neuronal stress-related molecules driving reactive astrogliosis in the peri-infarct cortex. MEM also blocks cortical spreading depression (Peeters et al., 2007), a phenomenon which induces astrogliosis (Sukhotinsky et al., 2011). It is possible that MEM-mediated inhibition of peri-infarct depolarizations (Lauritzen et al., 2011), which are electrophysiologically indistinguishable from spreading depression, might both reduce astrogliosis and favor improved recovery. It also cannot be ruled out that MEM had a direct effect on astrocytes.

Increased BDNF signaling.

BDNF has protean effects on the nervous system during development, plasticity, and injury repair(Schinder and Poo, 2000; Nagappan and Lu, 2005). Increases in BDNF expression have been reported in peri-infarct cortex after stroke and correlate with functional recovery; conversely, attenuation of BDNF activity worsens outcome (Chen et al., 2005; Sulejczak et al., 2007). MEM treatment at levels comparable to ours has been shown to increase BDNF mRNA expression across the brain (Marvanová et al., 2001; Molinaro et al., 2009).

We observed an increase in BDNF and p-TrkB expression in MEM- compared to vehicle-treated animals after stroke. This increase was specific to the infarcted hemisphere and it was significantly greater in MEM- than vehicle-treated animals. The specificity of the response suggests that signaling related to peri-infarct recovery and plasticity is relevant. The increase in MEM-treated animals suggests that MEM treatment may supplement an endogenous tendency to BDNF increase after stroke.

The mechanism of MEM-induced BDNF increase is not clear. A similar increase in BDNF and TrkB expression in rats treated with MK-801 suggests the BDNF increase might be NMDA-receptor associated (Marvanová et al., 2004; Guo et al., 2010; Al-Amin et al., 2011). However, though NMDA activity and BDNF secretion are often tightly linked in models of central nervous system plasticity; NMDA-associated BDNF-mediated plasticity is typically dependent on *activation*, not suppression, of NMDA receptor activity (Dietrich et al., 2000; Baumbauer et al., 2009; Chen et al., 2010; Ninan et al., 2010). One report suggests that MEM-induced BDNF changes are independent of its NMDA antagonism (Jantas et al., 2009).

Conclusions and translational relevance.

We have shown that chronic MEM treatment improves stroke outcome and sensory map recovery, in a manner that does not appear to be neuroprotective, and involves decreased reactive astrocytosis, increased vascular density, and increased BDNF expression. Because our findings affect behavior and anatomically specific functional maps, a neuronal mechanism for MEM's effects is obligatory, though it may not be the only one. MEM has been used for many years in treatment of Alzheimer's and other neurological diseases, and has proven well tolerated in an elderly, medically complex population. More recently, MEM has been used to successfully treat post-stroke aphasia (Berthier et al., 2009), showing that it is well tolerated in a post-stroke population, and effective in promoting post-stroke plasticity. Further evaluation of MEM's mechanisms in post stroke plasticity, and testing of MEM in clinical trials, may be warranted.

References

Al-Amin H, Sarkis R, Atweh S, Jabbur S, Saadé N (2011) Chronic dizocilpine or apomorphine and development of neuropathy in two animal models II: effects on brain cytokines and neurotrophins. Exp Neurol 228:30–40.

Babu CS, Ramanathan M (2009) Pre-ischemic treatment with memantine reversed the neurochemical and behavioural parameters but not energy metabolites in middle cerebral artery occluded rats. Pharmacol Biochem Behav 92:424–432.

Bacigaluppi M, Pluchino S, Peruzzotti-Jametti L, Jametti LP, Kilic E, Kilic U, Salani G, Brambilla E, West MJ, Comi G, Martino G, Hermann DM (2009) Delayed post-ischaemic neuroprotection following systemic neural stem cell transplantation involves multiple mechanisms. Brain 132:2239–2251.

Baumbauer KM, Huie JR, Hughes AJ, Grau JW (2009) Timing in the absence of supraspinal input II: regularly spaced stimulation induces a lasting alteration in spinal function that depends on the NMDA receptor, BDNF release, and protein synthesis. J Neurosci 29:14383–14393.

Benowitz LI, Carmichael ST (2010) Promoting axonal rewiring to improve outcome after stroke. Neurobiol Dis 37:259–266.

Berthier ML, Green C, Lara JP, Higueras C, Barbancho MA, Dávila G, Pulvermüller F (2009) Memantine and constraint-induced aphasia therapy in chronic poststroke aphasia. Ann Neurol 65:577–585.

Brown CE, Aminoltejari K, Erb H, Winship IR, Murphy TH (2009) In vivo voltage-sensitive dye imaging in adult mice reveals that somatosensory maps lost to stroke are replaced over weeks by new structural and functional circuits with prolonged modes of activation within both the peri-infarct zone and distant sites. J Neurosci 29:1719–1734.

Brown CE, Li P, Boyd JD, Delaney KR, Murphy TH (2007) Extensive turnover of dendritic spines and vascular remodeling in cortical tissues recovering from stroke. J Neurosci 27:4101–4109.

Carmichael ST (2010) Targets for neural repair therapies after stroke. Stroke 41:S124–126.

Chen H-SV, Lipton SA (2006) The chemical biology of clinically tolerated NMDA receptor antagonists. J Neurochem 97:1611–1626.

Chen J, Zacharek A, Zhang C, Jiang H, Li Y, Roberts C, Lu M, Kapke A, Chopp M (2005) Endothelial nitric oxide synthase regulates brain-derived neurotrophic factor expression and neurogenesis after stroke in mice. J Neurosci 25:2366–2375.

Chen LY, Rex CS, Pham DT, Lynch G, Gall CM (2010) BDNF signaling during learning is regionally differentiated within hippocampus. J Neurosci 30:15097–15101.

Chen, Wang YF, Rayudu PV, Edgecomb P, Neill JC, Segal MM, Lipton SA, Jensen FE (1998) Neuroprotective concentrations of the N-methyl-D-aspartate open-channel blocker memantine are effective without cytoplasmic vacuolation following post-ischemic administration and do not block maze learning or long-term potentiation. Neuroscience 86:1121–1132.

Clarkson A, Lopez-Valdes H, Overman J, Charles A, Brennan K, Carmichael S (2013) Multimodal examination of structural and functional remapping in the mouse photothrombotic stroke model. J Cereb Blood Flow Metab In Press.

Clarkson AN, Huang BS, Macisaac SE, Mody I, Carmichael ST (2010) Reducing excessive GABA-mediated tonic inhibition promotes functional recovery after stroke. Nature 468:305–309.

Clarkson AN, Overman JJ, Zhong S, Mueller R, Lynch G, Carmichael ST (2011) AMPA receptor-induced local brain-derived neurotrophic factor signaling mediates motor recovery after stroke. J Neurosci 31:3766–3775.

David-Jürgens M, Churs L, Berkefeld T, Zepka RF, Dinse HR (2008) Differential effects of aging on fore- and hindpaw maps of rat somatosensory cortex. PLoS ONE 3:e3399.

Dietrich WD, Truettner J, Prado R, Stagliano NE, Zhao W, Busto R, Ginsberg MD, Watson BD (2000) Thromboembolic events lead to cortical spreading depression and expression of c-fos, brain-derived neurotrophic factor, glial fibrillary acidic protein, and heat shock protein 70 mRNA in rats. J Cereb Blood Flow Metab 20:103–111.

Frostig RD, Lieke EE, Ts'o DY, Grinvald A (1990) Cortical functional architecture and local coupling between neuronal activity and the microcirculation revealed by in vivo high-resolution optical imaging of intrinsic signals. Proc Natl Acad Sci U S A 87:6082–6086.

Görgülü A, Kinş T, Cobanoglu S, Unal F, Izgi NI, Yanik B, Küçük M (2000) Reduction of edema and infarction by Memantine and MK-801 after focal cerebral ischaemia and reperfusion in rat. Acta Neurochir (Wien) 142:1287–1292.

Grinvald A, Lieke E, Frostig RD, Gilbert CD, Wiesel TN (1986) Functional architecture of cortex revealed by optical imaging of intrinsic signals. Nature 324:361–364.

Guo C, Yang Y, Su Y, Si T (2010) Postnatal BDNF expression profiles in prefrontal cortex and hippocampus of a rat schizophrenia model induced by MK-801 administration. J Biomed Biotechnol 2010:783297.

Hao J, Mdzinarishvili A, Abbruscato TJ, Klein J, Geldenhuys WJ, Van der Schyf CJ, Bickel U (2008) Neuroprotection in mice by NGP1-01 after transient focal brain ischemia. Brain Res 1196:113–120.

Hardingham GE, Bading H (2010) Synaptic versus extrasynaptic NMDA receptor signalling: implications for neurodegenerative disorders. Nat Rev Neurosci 11:682–696.

Jantas D, Szymanska M, Budziszewska B, Lason W (2009) An involvement of BDNF and PI3-K/Akt in the anti-apoptotic effect of memantine on staurosporine-evoked cell death in primary cortical neurons. Apoptosis 14:900–912.

Johnson JW, Kotermanski SE (2006) Mechanism of action of memantine. Curr Opin Pharmacol 6:61–67.

Jones TA, Allred RP, Adkins DL, Hsu JE, O'Bryant A, Maldonado MA (2009) Remodeling the Brain With Behavioral Experience After Stroke. Stroke 40:S136–S138.

Ke Z, Yip SP, Li L, Zheng X-X, Tong K-Y (2011) The effects of voluntary, involuntary, and forced exercises on brain-derived neurotrophic factor and motor function recovery: a rat brain ischemia model. PLoS ONE 6:e16643.

Kermani P, Hempstead B (2007) Brain-derived neurotrophic factor: a newly described mediator of angiogenesis. Trends Cardiovasc Med 17:140–143.

Kilkenny C, Browne WJ, Cuthill IC, Emerson M, Altman DG (2010) Improving Bioscience Research Reporting: The ARRIVE Guidelines for Reporting Animal Research. PLoS Biol 8:e1000412.

Kinlay S (2011) Changes in stroke epidemiology, prevention, and treatment. Circulation 124:e494–496.

Kleim JA, Boychuk JA, Adkins DL (2007) Rat models of upper extremity impairment in stroke. ILAR J 48:374–384.

Kornhuber J, Quack G (1995) Cerebrospinal fluid and serum concentrations of the N-methyl-D-aspartate (NMDA) receptor antagonist memantine in man. Neurosci Lett 195:137–139.

Landis SC et al. (2012) A call for transparent reporting to optimize the predictive value of preclinical research. Nature 490:187–191.

Lapchak PA (2006) Memantine, an uncompetitive low affinity NMDA open-channel antagonist improves clinical rating scores in a multiple infarct embolic stroke model in rabbits. Brain Res 1088:141–147.

Lauritzen M, Dreier JP, Fabricius M, Hartings JA, Graf R, Strong AJ (2011) Clinical relevance of cortical spreading depression in neurological disorders: migraine, malignant stroke, subarachnoid and intracranial hemorrhage, and traumatic brain injury. J Cereb Blood Flow Metab 31:17–35.

Li S, Overman JJ, Katsman D, Kozlov SV, Donnelly CJ, Twiss JL, Giger RJ, Coppola G, Geschwind DH, Carmichael ST (2010) An age-related sprouting transcriptome provides molecular control of axonal sprouting after stroke. Nat Neurosci 13:1496–1504.

Li X, Blizzard KK, Zeng Z, DeVries AC, Hurn PD, McCullough LD (2004) Chronic behavioral testing after focal ischemia in the mouse: functional recovery and the effects of gender. Exp Neurol 187:94–104.

Li Y, Chen J, Zhang CL, Wang L, Lu D, Katakowski M, Gao Q, Shen LH, Zhang J, Lu M, Chopp M (2005) Gliosis and brain remodeling after treatment of stroke in rats with marrow stromal cells. Glia 49:407–417.

Liu C, Lin N, Wu B, Qiu Y (2009) Neuroprotective effect of memantine combined with topiramate in hypoxic-ischemic brain injury. Brain Res 1282:173–182.

Martinez-Coria H, Green KN, Billings LM, Kitazawa M, Albrecht M, Rammes G, Parsons CG, Gupta S, Banerjee P, LaFerla FM (2010) Memantine improves cognition and reduces Alzheimer's-like neuropathology in transgenic mice. Am J Pathol 176:870–880.

Marvanová M, Lakso M, Pirhonen J, Nawa H, Wong G, Castrén E (2001) The neuroprotective agent memantine induces brain-derived neurotrophic factor and trkB receptor expression in rat brain. Mol Cell Neurosci 18:247–258.

Marvanová M, Lakso M, Wong G (2004) Identification of genes regulated by memantine and MK-801 in adult rat brain by cDNA microarray analysis. Neuropsychopharmacology 29:1070–1079.
Meisner F, Scheller C, Kneitz S, Sopper S, Neuen-Jacob E, Riederer P, Ter Meulen V, Koutsilieri E (2008) Memantine upregulates BDNF and prevents dopamine deficits in SIV-infected macaques: a novel pharmacological action of memantine. Neuropsychopharmacology 33:2228–2236.
Minkeviciene R, Banerjee P, Tanila H (2004) Memantine improves spatial learning in a transgenic mouse model of Alzheimer's disease. J Pharmacol Exp Ther 311:677–682.
Molinaro G, Battaglia G, Riozzi B, Di Menna L, Rampello L, Bruno V, Nicoletti F (2009) Memantine treatment reduces the expression of the K(+)/Cl(-) cotransporter KCC2 in the hippocampus and cerebral cortex, and attenuates behavioural responses mediated by GABA(A) receptor activation in mice. Brain Res 1265:75–79.
Murphy TH, Corbett D (2009) Plasticity during stroke recovery: from synapse to behaviour. Nat Rev Neurosci 10:861–872.
Myer DJ, Gurkoff GG, Lee SM, Hovda DA, Sofroniew MV (2006) Essential protective roles of reactive astrocytes in traumatic brain injury. Brain 129:2761–2772.
Nagappan G, Lu B (2005) Activity-dependent modulation of the BDNF receptor TrkB: mechanisms and implications. Trends Neurosci 28:464–471.
Ninan I, Bath KG, Dagar K, Perez-Castro R, Plummer MR, Lee FS, Chao MV (2010) The BDNF Val66Met polymorphism impairs NMDA receptor-dependent synaptic plasticity in the hippocampus. J Neurosci 30:8866–8870.
Ohab JJ, Fleming S, Blesch A, Carmichael ST (2006) A neurovascular niche for neurogenesis after stroke. J Neurosci 26:13007–13016.
Peeters M, Gunthorpe MJ, Strijbos PJ, Goldsmith P, Upton N, James MF (2007) Effects of pan- and subtype-selective NMDA receptor antagonists on cortical spreading depression in the rat: therapeutic potential for migraine. J Pharmacol Exp Ther 321:564–572.
Ploughman M, Windle V, MacLellan CL, White N, Doré JJ, Corbett D (2009) Brain-derived neurotrophic factor contributes to recovery of skilled reaching after focal ischemia in rats. Stroke 40:1490–1495.
Qin L, Kim E, Ratan R, Lee FS, Cho S (2011) Genetic variant of BDNF (Val66Met) polymorphism attenuates stroke-induced angiogenic responses by enhancing anti-angiogenic mediator CD36 expression. J Neurosci 31:775–783.
Ramanathan D, Conner JM, Tuszynski MH (2006) A form of motor cortical plasticity that correlates with recovery of function after brain injury. Proc Natl Acad Sci USA 103:11370–11375.
Rammes G, Danysz W, Parsons CG (2008) Pharmacodynamics of memantine: an update. Curr Neuropharmacol 6:55–78.
Rasband WS (1997) ImageJ, US National Institutes of Health, Bethesda, Maryland, USA. Available at: http://imagej.nih.gov/ij/.
Roger VL et al. (2012) Executive summary: heart disease and stroke statistics--2012 update: a report from the american heart association. Circulation 125:188–197.
Schallert T, Fleming SM, Leasure JL, Tillerson JL, Bland ST (2000) CNS plasticity and assessment of forelimb sensorimotor outcome in unilateral rat models of stroke, cortical ablation, parkinsonism and spinal cord injury. Neuropharmacology 39:777–787.
Schinder AF, Poo M (2000) The neurotrophin hypothesis for synaptic plasticity. Trends Neurosci 23:639–645.
Shih AY, Blinder P, Tsai PS, Friedman B, Stanley G, Lyden PD, Kleinfeld D (2013) The smallest stroke: occlusion of one penetrating vessel leads to infarction and a cognitive deficit. Nat Neurosci 16:55–63.
Sofroniew MV (2009) Molecular dissection of reactive astrogliosis and glial scar formation. Trends Neurosci 32:638–647.
Sukhotinsky I, Dilekoz E, Wang Y, Qin T, Eikermann-Haerter K, Waeber C, Ayata C (2011) Chronic daily cortical spreading depressions suppress spreading depression susceptibility. Cephalalgia 31:1601–1608.
Sulejczak D, Ziemlińska E, Czarkowska-Bauch J, Nosecka E, Strzalkowski R, Skup M (2007) Focal photothrombotic lesion of the rat motor cortex increases BDNF levels in motor-sensory cortical areas not accompanied by recovery of forelimb motor skills. J Neurotrauma 24:1362–1377.

Tennant KA, Adkins DL, Donlan NA, Asay AL, Thomas N, Kleim JA, Jones TA (2011) The organization of the forelimb representation of the C57BL/6 mouse motor cortex as defined by intracortical microstimulation and cytoarchitecture. Cereb Cortex 21:865–876.

Thomas SJ, Grossberg GT (2009) Memantine: a review of studies into its safety and efficacy in treating Alzheimer's disease and other dementias. Clin Interv Aging 4:367–377.

Xia P, Chen HV, Zhang D, Lipton SA (2010) Memantine preferentially blocks extrasynaptic over synaptic NMDA receptor currents in hippocampal autapses. J Neurosci 30:11246–11250.

Zhang ZG, Chopp M (2009) Neurorestorative therapies for stroke: underlying mechanisms and translation to the clinic. Lancet Neurol 8:491–500.

Figure Legends

Figure 1. Experimental design and animal preparation. A. Schematic shows temporal sequence of stroke and experimental modalities. B. Image shows intact translucent mouse skull oriented for imaging. Green circle shows area exposed to photothrombosis; white and black squares show regions of interest for forepaw (FP) and hindpaw (HP) OIS map analysis. Inside the regions of interest are FP (purple) and HP (yellow) activation maps. Red lines show boundaries of tissue removed for Western blot analysis.

Figure 2. Post-stroke memantine treatment is not neuroprotective. A,B. Representative 40 μm Nissl stained sections collected 7 days after infarct for vehicle- and MEM-treated animals, respectively. C. shows mean (± SEM) infarct area (in mm3; 4 animals per group). There was no significant difference in infarct area. D, E, F. Representative NeuN stained sections from sham stroke-, vehicle-, and MEM-treated animals, respectively. A1-A6: regions of interest; *: infarct core. G. Percent area occupied by NeuN-positive cells in 250μm wide regions of interest at increasing distances from infarct core (or equivalent location in sham-stroke-treated animals). There was no significant difference in area between groups. H. Average area of NeuN-positive cells in region of interest closest to infarct (Area 1; n (putative cells) = 245 control, 214 Stroke + Vehicle, 248 Stroke + MEM). Both vehicle- and MEM-treated animals showed an increase in average cell size compared to sham-treated animals, but there was no significant difference between the two groups (One-way ANOVA with Newman-Keuls Multiple Comparison Test; N.S.: not significant).

Figure 3. Improved behavioral recovery from stroke with MEM treatment. A. Cylinder test. Graph shows spontaneous forepaw asymmetry index, which records paw use on rearing (Index=(Left–Right)/(Left+Right+simultaneous). The animals were recorded for 10 minutes and the impaired limb was on the right side. There was a significant improvement in forepaw asymmetry at 28 days of MEM treatment (***$p<0.001$; Repeated-measures One-Way ANOVA with Newman–Keuls' multiple pair-wise comparisons; 6 animals per group). B, C. Grid-Walking test. Functional recovery was assessed with forelimb (B) and hindlimb (C) foot faults. There was a significant reduction in forelimb but not hindlimb foot faults at 28 days of MEM

treatment ($p<0.05$, two-way ANOVA with repeated measures and Newman–Keuls' multiple pair-wise comparisons, 6 animals per group).

Figure 4. Significant recovery of forepaw sensory maps with MEM treatment. A. FP and HP sensory maps in representative vehicle (Stroke +Veh) and MEM (Stroke +Mem) treated animals , recorded 7 days before (-7), and 7, 14, 21 and 28 after photothrombosis. Last column shows overlay of pre-stroke and 28 day post-stroke maps. B, C. Area of activation (mean±SEM, half maximal signal) for FP and HP respectively. There was a significant increase in FP, but not HP, activation area at 28 days of MEM treatment (*$p<0.05$, One-way repeated measures ANOVA with Tukey Multiple Comparison Test, 6 animals per group).

Figure 5. Decreased reactive astrocytosis in MEM-treated animals. A,B, C. Representative GFAP inmuhistochemistry from sham stroke-, vehicle- and MEM-treated groups respectively. A1-6: regions of interest; *: infarct core; arrows: glial scar. D. Percent area occupied by GFAP-positive cells, in 250μm wide regions of interest beginning at the margin of the glial scar. There was a significant reduction in percent area occupied by GFAP-positive cells in MEM- compared to vehicle-treated animals. There was no significant difference in the area of the glial scar between MEM- and vehicle-treated animals (Inset)(One-way ANOVA with Tukey Multiple Comparison Test *$p<0.05$, **$p<0.01$, ***$p<0.001$; 4 animals per group).

Figure 6. Increased vascular density in MEM-treated animals. A, B, C. Color figures show representative PECAM-1 inmuhistochemistry for sham stroke-, vehicle- and MEM-treated animals, respectively. The color insert in each figure is an amplification. Black and white figures in each panel are the same figures after image processing. D, E. PECAM-1 quantification. D. shows percent area occupied by PECAM-1 inmunoreactivity in 250μm wide regions of interest beginning at the glial scar margin (a proxy for vascular density); E. shows the average area of each PECAM-1-positive image region (a proxy for vascular length and diameter). There was a significant difference in both measures between MEM-and vehicle-treated animals (One way ANOVA with Bonferroni post hoc testing; *$p<0.05$, **$p<0.01$, ***$p<0.001$; 4 animals per group).

Figure 7. Increased BNDF pathway signaling in MEM-treated animals. A. Quantification (mean optical density, normalized to GADPH) of Western Blots (representative blots in B.). There was a significant increase in BDNF and phospho-TrkB expression, consistent with activation of the BDNF pathway. (*$p<0.05$, Student's t test; 4-6 animals per group).

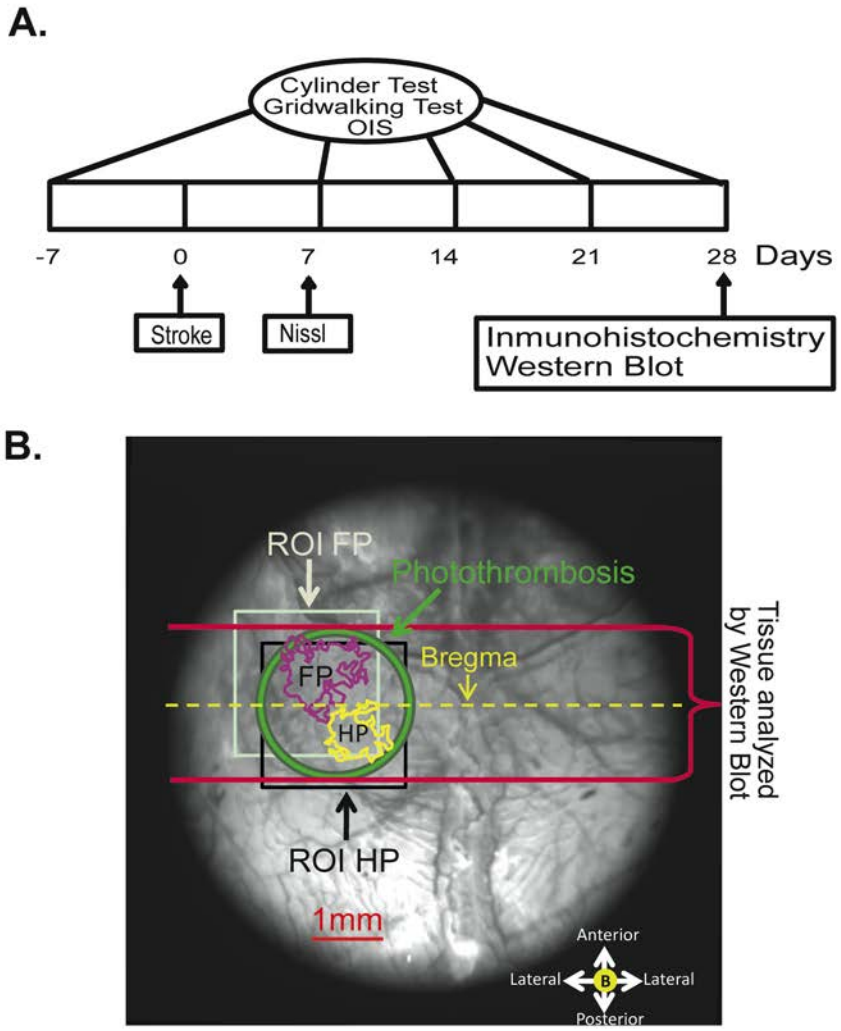

Figure 1. Experimental design and animal preparation. A. Schematic shows temporal sequence of stroke and experimental modalities. B. Image shows intact translucent mouse skull oriented for imaging. Green circle shows area exposed to photothrombosis; white and black squares show regions of interest for forepaw (FP) and hindpaw (HP) OIS map analysis. Inside the regions of interest are FP (purple) and HP (yellow) activation maps. Red lines show boundaries of tissue removed for Western blot analysis.

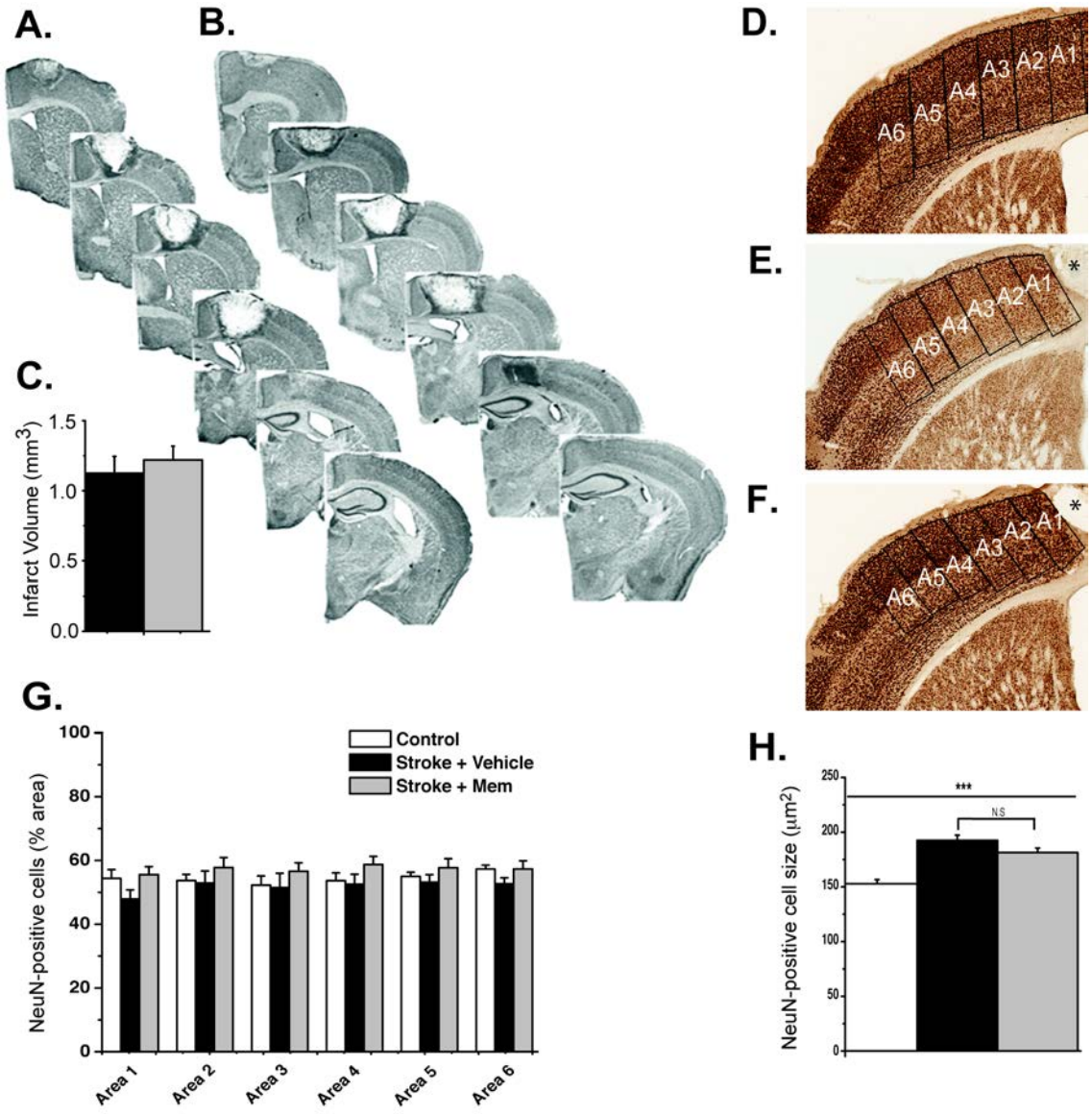

Figure 2. Post-stroke memantine treatment is not neuroprotective. A,B. Representative 40 μm Nissl stained sections collected 7 days after infarct for vehicle- and MEM-treated animals, respectively. C. shows mean (± SEM) infarct area (in mm3; 4 animals per group). There was no significant difference in infarct area. D, E, F. Representative NeuN stained sections from sham stroke-, vehicle-, and MEM-treated animals, respectively. A1-A6: regions of interest; *: infarct core. G. Percent area occupied by NeuN-positive cells in 250μm wide regions of interest at increasing distances from infarct core (or equivalent location in sham-stroke-treated animals). There was no significant difference in area between groups. H. Average area of NeuN-positive cells in region of interest closest to infarct (Area 1; n (putative cells) = 245 control, 214 Stroke + Vehicle, 248 Stroke + MEM). Both vehicle- and MEM-treated animals showed an increase in average cell size compared to sham-treated animals, but there was no significant difference between the two groups (One-way ANOVA with Newman-Keuls Multiple Comparison Test; N.S.: not significant).

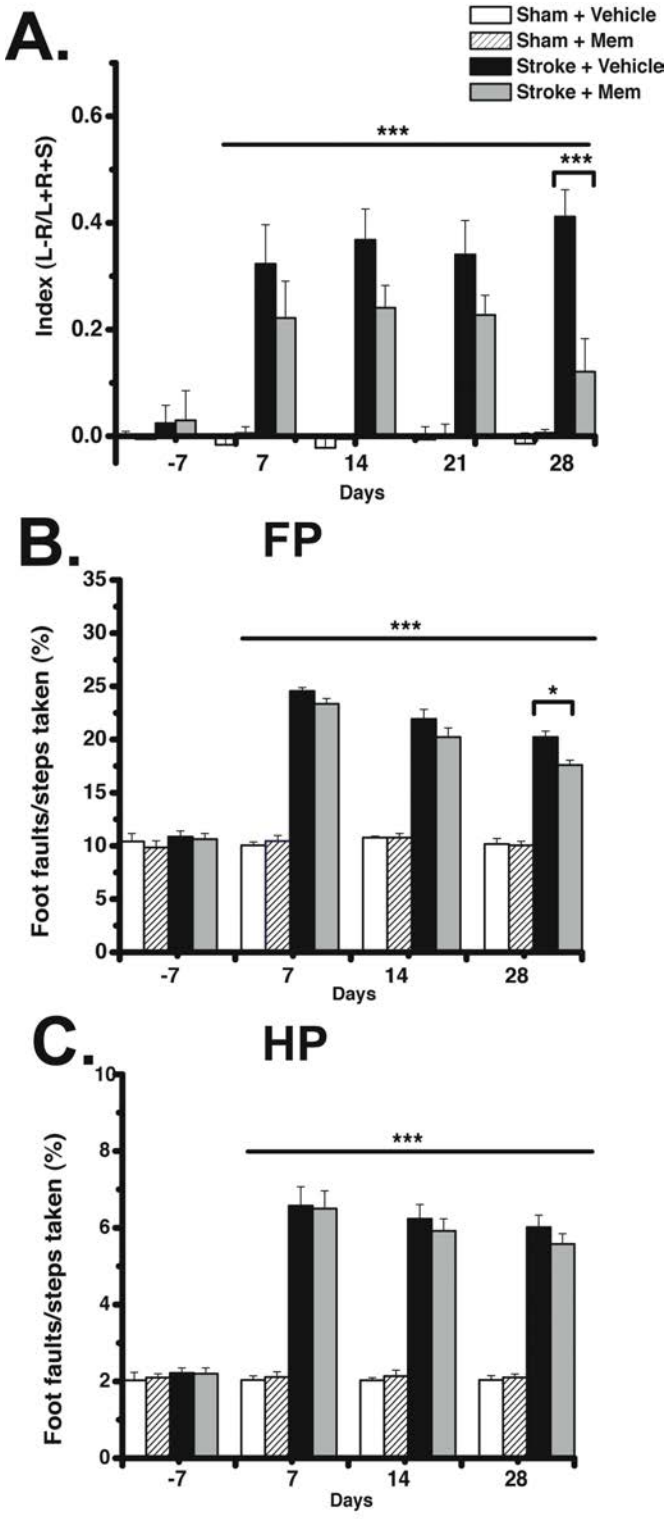

Figure 3. Improved behavioral recovery from stroke with MEM treatment. A. Cylinder test. Graph shows spontaneous forepaw asymmetry index, which records paw use on rearing (Index=(Left–Right)/(Left+Right+simultaneous). The animals were recorded for 10 minutes and the impaired limb was on the right side. There was a significant improvement in forepaw asymmetry at 28 days of MEM treatment (***$p<0.001$; Repeated-measures One-Way ANOVA with Newman–Keuls' multiple pair-wise comparisons; 6 animals per group). B, C. Grid-Walking test. Functional recovery was assessed with forelimb (B) and hindlimb (C) foot faults. There was a significant reduction in forelimb but not hindlimb foot faults at 28 days of MEM treatment ($p<0.05$, two-way ANOVA with repeated measures and Newman–Keuls' multiple pair-wise comparisons, 6 animals per group).

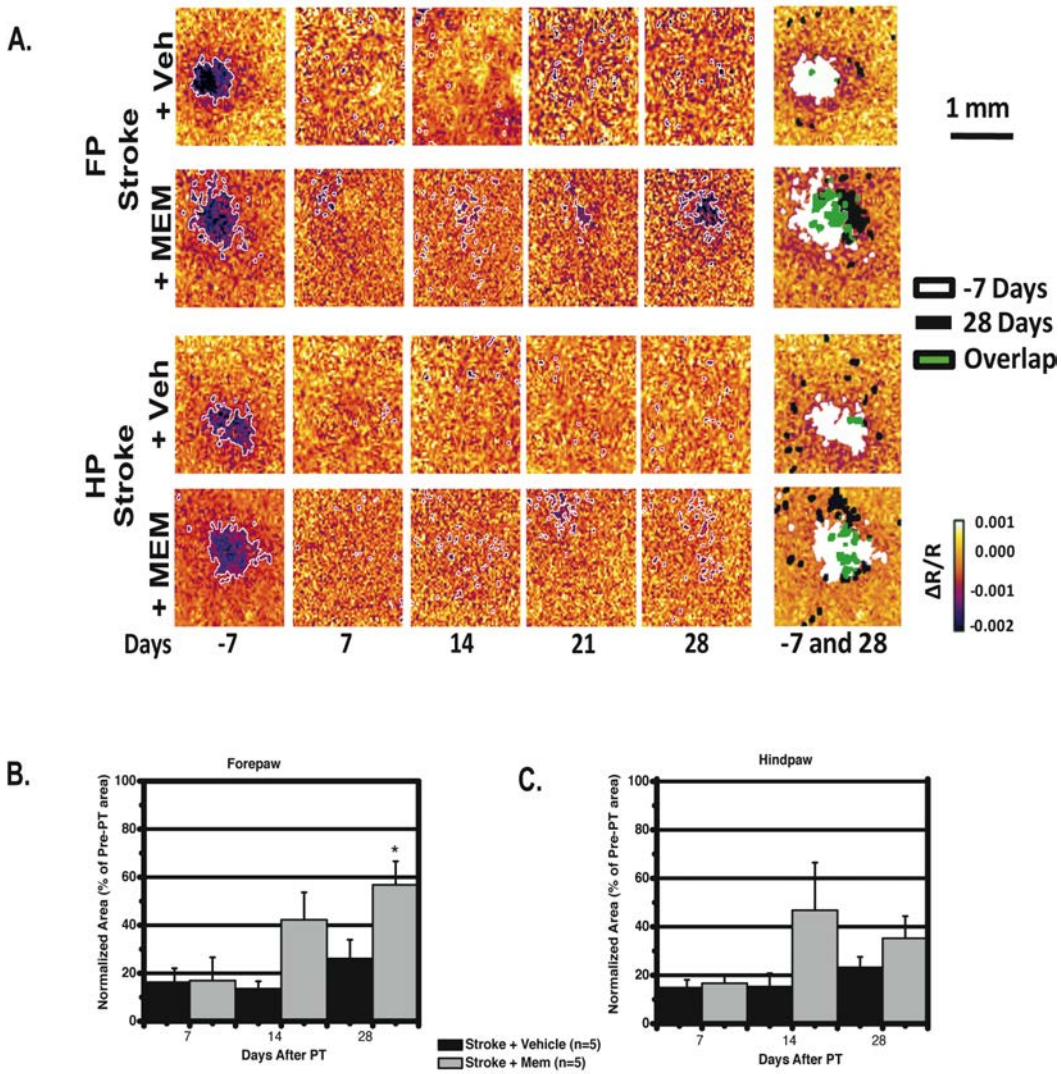

Figure 4. Significant recovery of forepaw sensory maps with MEM treatment. A. FP and HP sensory maps in representative vehicle (Stroke +Veh) and MEM (Stroke +Mem) treated animals , recorded 7 days before (-7), and 7, 14, 21 and 28 after photothrombosis. Last column shows overlay of pre-stroke and 28 day post-stroke maps. B, C. Area of activation (mean±SEM, half maximal signal) for FP and HP respectively. There was a significant increase in FP, but not HP, activation area at 28 days of MEM treatment (*$p<0.05$, One-way repeated measures ANOVA with Tukey Multiple Comparison Test, 6 animals per group).

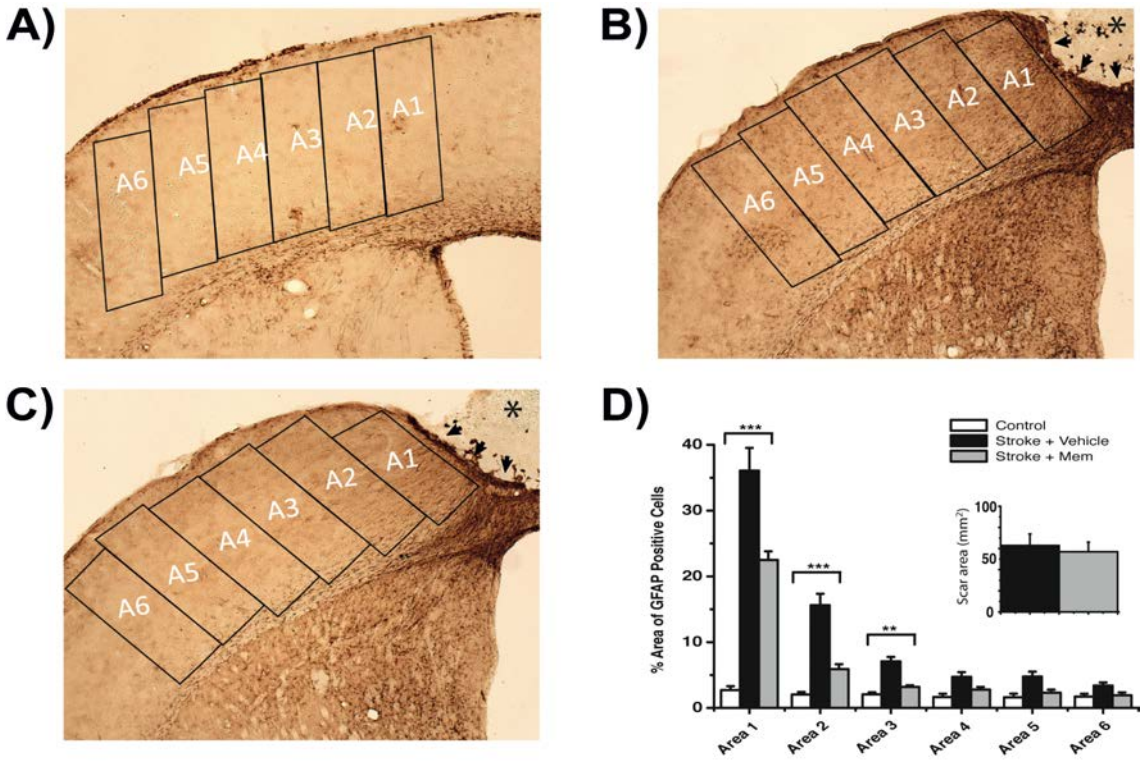

Figure 5. Decreased reactive astrocytosis in MEM-treated animals. A,B, C. Representative GFAP inmuhistochemistry from sham stroke-, vehicle- and MEM-treated groups respectively. A1-6: regions of interest; *: infarct core; arrows: glial scar. D. Percent area occupied by GFAP-positive cells, in 250μm wide regions of interest beginning at the margin of the glial scar. There was a significant reduction in percent area occupied by GFAP-positive cells in MEM- compared to vehicle-treated animals. There was no significant difference in the area of the glial scar between MEM- and vehicle-treated animals (Inset)(One-way ANOVA with Tukey Multiple Comparison Test *$p<0.05$, **$p<0.01$, ***$p<0.001$; 4 animals per group).

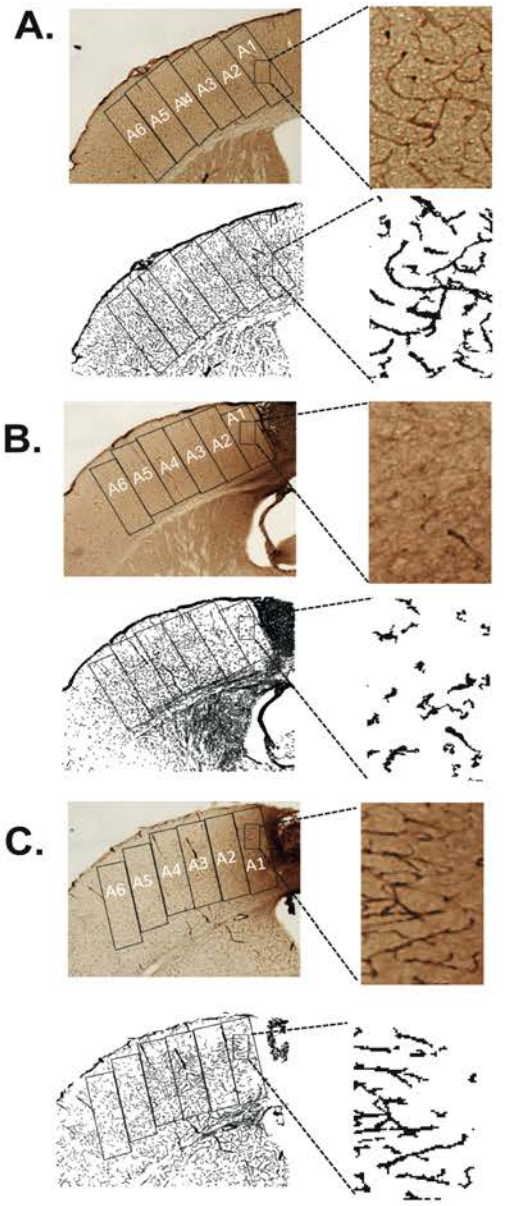

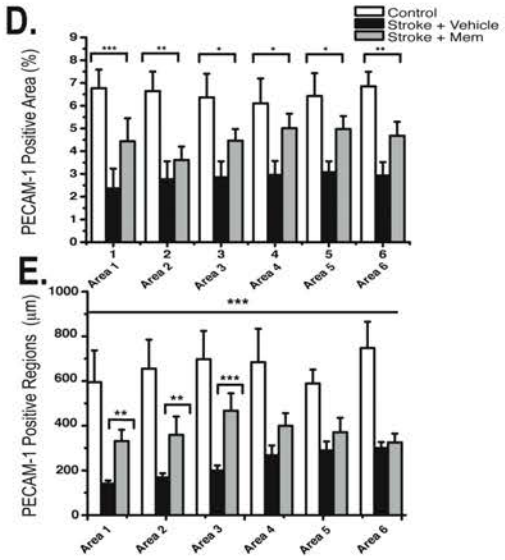

Figure 6. Increased vascular density in MEM-treated animals. A, B, C. Color figures show representative PECAM-1 inmuhistochemistry for sham stroke-, vehicle- and MEM-treated animals, respectively. The color insert in each figure is an amplification. Black and white figures in each panel are the same figures after image processing. D, E. PECAM-1 quantification. D. shows percent area occupied by PECAM-1 inmunoreactivity in 250µm wide regions of interest beginning at the glial scar margin (a proxy for vascular density); E. shows the average area of each PECAM-1-positive image region (a proxy for vascular length and diameter). There was a significant difference in both measures between MEM-and vehicle-treated animals (One way ANOVA with Bonferroni post hoc testing; *p<0.05, **p<0.01, ***p<0.001; 4 animals per group).

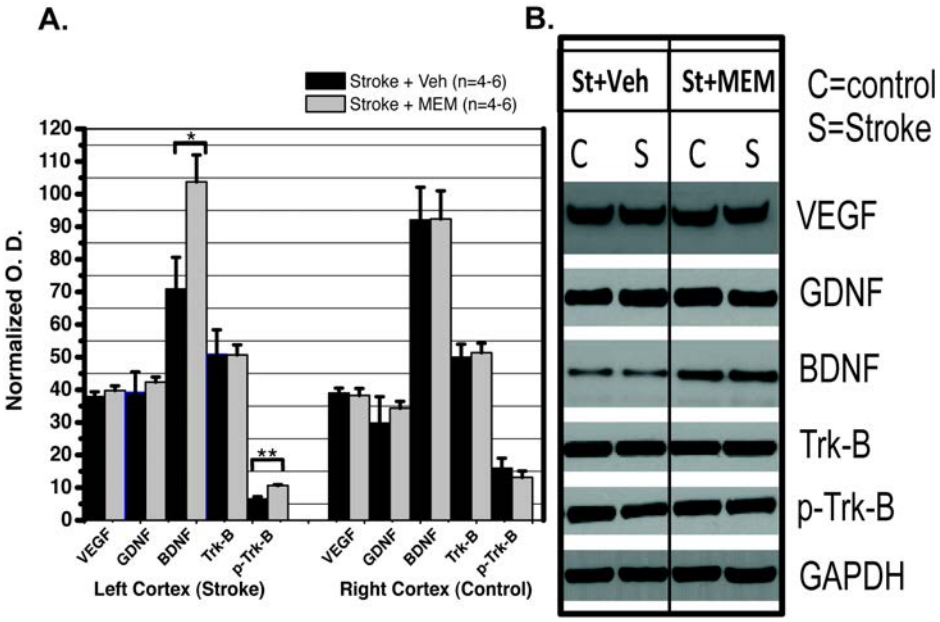

Figure 7. Increased BNDF pathway signaling in MEM-treated animals. A. Quantification (mean optical density, normalized to GADPH) of Western Blots (representative blots in B.). There was a significant increase in BDNF and phospho-TrkB expression, consistent with activation of the BDNF pathway. (*$p<0.05$, Student's t test; 4-6 animals per group).